



Contributions of natural and anthropogenic sources to ambient ammonia in the Athabasca Oil Sands and north-western Canada

Cynthia Whaley¹, Paul A. Makar¹, Mark W. Shephard¹, Leiming Zhang¹, Junhua Zhang¹, Qiong Zheng¹, Ayodeji Akingunola¹, Gregory R. Wentworth^{2,3}, Jennifer G. Murphy², Shailesh K. Kharol¹, and Karen E. Cady-Pereira⁴

¹Air Quality Research Division, Environment and Climate Change Canada, 4905 Dufferin Street, Toronto, Ontario, Canada

²Dept of Chemistry, University of Toronto, 80 St George Street, Toronto, Ontario, Canada

³Environmental Monitoring and Science Division, Alberta Environment and Parks, 9888 Jasper Ave NW, Edmonton, Alberta, Canada

⁴Atmospheric and Environmental Research (AER), Lexington, Massachusetts, USA

Correspondence to: Cynthia Whaley (cynthia.whaley@canada.ca)

Abstract. Atmospheric ammonia (NH_3) is a short-lived pollutant that plays an important role in aerosol chemistry and nitrogen deposition. Dominant NH_3 emissions are from agriculture and forest fires, both of which are increasing globally. The Alberta Oil Sands region has relatively low ambient NH_3 concentrations because of its remote location in northern Canada; however, a previous attempt

5 to model NH_3 in the region showed a substantial negative bias compared to satellite column and aircraft observations. Known missing sources of NH_3 in the model were re-emission of NH_3 from plants and soils (bidirectional flux), and forest fire emissions, but the relative impact of these sources on NH_3 concentrations and column totals was unknown. Here we have used a research version of the high-resolution air quality forecasting model, GEM-MACH, to quantify the relative impacts of

10 natural (bidirectional flux of NH_3 and forest fire emissions) and anthropogenic (Oil Sands operations, combustion of fossil fuels, and agriculture) sources on ammonia concentrations, both at the surface and aloft, with a focus on the Athabasca Oil Sands region, during a measurement-intensive campaign in the summer of 2013. The addition of fires and bidirectional flux has improved the model bias, slope and correlation coefficients relative to ground, aircraft, and satellite measurements significantly. By

15 running the GEM-MACH model in three configurations and calculating their differences, we find that averaged over Alberta and Saskatchewan during this time period; an average of 23.1% of surface NH_3 came from direct anthropogenic sources, 56.6% (or 1.24 ppbv) from bidirectional flux (re-emission from plants and soils), and 20.3% (or 0.42 ppbv) from forest fires. In the NH_3 total column, an average of 19.5% came from direct anthropogenic sources, 50.0% from bidirectional flux, and

20 30.5% from forest fires. The addition of bidirectional flux and fire emissions caused the overall average net flux of NH_3 across the domain to be positive (upward). It also increased the NH_4^+ wet



deposition by nearly a factor of three during the period simulated. Note that forest fires are very episodic and their contributions will vary significantly for different time periods and regions.

1 Introduction

25 Ammonia (NH_3) is a short-lived pollutant that is receiving global attention because of its increasing concentrations. Emissions of NH_3 – which are in large part from agricultural fertilizer, livestock (Behera et al., 2013; Environment and Climate Change Canada, 2016), and biomass burning (Olivier et al., 1998; Krupa, 2003) – have not been regulated to the same extent as other nitrogen species. NH_3 is the only aerosol precursor whose global emissions are projected to rise throughout
30 the next century (Moss et al., 2010; Lamarque et al., 2010; Ciais et al., 2013).

NH_3 has an atmospheric lifetime of hours to a day (Seinfeld and Pandis, 1998; Aneja et al., 2001). It is a base that reacts in the atmosphere with sulphuric acid (H_2SO_4) and nitric acid (HNO_3) to form crystalline sulphate, nitrate salts (e.g., $(\text{NH}_4)_2\text{SO}_4$, NH_4HSO_4 , NH_4NO_3) and aqueous ions (SO_4^{2-} , HSO_4^- , NO_3^-), (Nenes et al., 1998; Makar et al., 2003) which are significant components of
35 fine particulate matter ($\text{PM}_{2.5}$) (e.g., Jimenez et al., 2009), thus causing health (Pope III et al., 2002; Lee et al., 2015) and climate impacts (IPCC, 2013). A large portion of NH_3 is readily deposited in the first 4-5 km from its source, but when in fine particulate form (as NH_4^+), its lifetime is days to several weeks (Galperin and Sofiev, 1998; Park et al., 2004; Behera et al., 2013; Paulot et al., 2014) and can be transported hundreds of kilometers (Krupa, 2003; Galloway et al., 2008; Makar et al.,
40 2009). Deposition of NH_3 and these aerosols can lead to nitrogen eutrophication and soil acidification (Fangmeier et al., 1994; Sutton et al., 1998; Dragosits et al., 2002; Carfrae et al., 2004). Thus, NH_3 is listed as a Criteria Air Contaminant (Environment and Climate Change Canada, 2017) in order to help address air quality issues such as smog and acid rain.

Modelling provides information on NH_3 concentrations where there are no measurements, and can
45 be used to better understand NH_3 processes. Recent NH_3 models have focused on improving bidirectional flux processes and impacts of livestock. Measurements of NH_3 bidirectional flux include those in Farquhar et al. (1980); Sutton et al. (1993, 1995); Asman et al. (1998); Nemitz et al. (2001), with indirect support for bidirectional flux also in Ellis et al. (2011). Thus, these studies were the motivation for the recent design of parameterizations to describe this important process (Wu et al., 2009;
50 Wichink Kruit et al., 2010; Massad et al., 2010; Zhang et al., 2010; Zhu et al., 2015; Fu et al., 2015; Hansen et al., 2017). Additionally, satellite observations are providing valuable insight on ammonia concentrations and emissions both on regional and global scales (Beer et al., 2008; Clarisse et al., 2009; Shephard et al., 2011; Shephard and Cady-Pereira, 2015; Van Damme et al., 2014; Zhu et al., 2013).

55 The Athabasca Oil Sands region (AOSR), located in the province of Alberta, Canada, is a large source of air (Gordon et al., 2015; Liggio et al., 2016; Li et al., 2017), ecosystem (Kelly et al., 2009;



Kirk et al., 2014; Hsu and Clair, 2015) and greenhouse gas (Charpentier et al., 2009) pollution due to mining and processing by the oil industry. However NH_3 concentrations in northern Alberta and Saskatchewan remain relatively low (e.g., averaging 0.63 ± 0.57 ppbv at the surface, (this study); and averaging 1.2 ± 0.2 ppbv aloft (Shephard et al., 2015) compared to agricultural areas in the south of the provinces (e.g., Makar et al., 2009). However, a monitoring study from 2005 to 2008 found NH_3 concentrations near Fort McMurray and Fort McKay (population centers in the vicinity of the oil sands facilities) to be highly variable in space and time with a range of 1.1 to 8.8 ppbv (Bytnerowicz et al., 2010). NH_3 may contribute the largest fraction of deposited nitrogen in the AOSR compared to other nitrogen species like NO_2 and HNO_3^- (Bytnerowicz et al., 2010; Hsu and Clair, 2015; Kharol et al., 2017). Estimates of deposition of nitrogen and sulphur compounds in the AOSR are described in Makar et al. (2017) in this issue.

In a previous study by Shephard et al. (2015) it was found that the GEM-MACH air quality forecasting model (Moran et al., 2010, 2013; Makar et al., 2015a, b; Gong et al., 2015), using a domain covering the Canadian provinces of Alberta and Saskatchewan, at 2.5-km resolution, under-predicted tropospheric ammonia concentrations by 0.4-0.6 ppbv (36-100 % depending on altitude - see Fig. 16 in Shephard et al., 2015) in the AOSR when compared to Tropospheric Emission Spectrometer (TES) satellite measurements and aircraft measurements. NH_3 sources known to be missing from the GEM-MACH model were forest fire emissions and re-emission of deposited NH_3 from soils and plants (the latter referred to as bidirectional flux, hereafter). These two sources were added to an updated version of GEM-MACH and model simulations were repeated for a 2013 summer period (12 August to 7 September 2013) during which an intensive measurement campaign occurred. We utilize ground, aircraft and satellite measurements of NH_3 and related species to evaluate the model and to quantify the impacts of the different sources on atmospheric NH_3 and its deposition.

Section 2 provides the model description. Section 3 provides a brief description of ammonia measurements during the campaign. Section 4 presents the evaluation of three model scenarios against three different types of measurements (surface, aircraft, and satellite), and Section 5 presents our quantitative assessment on the impacts of different sources of NH_3 to ambient concentrations in the region. Our conclusions appear in Section 6.

2 GEM-MACH model description

GEM-MACH (Global Environment Multiscale-Modelling Air quality and CHemistry) is an on-line chemical transport model, which is embedded in GEM, Environment and Climate Change Canada's numerical weather prediction model (Moran et al., 2010). This means that the chemical processes of the model (gas-phase chemistry, plume rise emissions distribution, vertical diffusion and surface fluxes of tracers, and a particle chemistry package including particle microphysics, cloud processes, and inorganic heterogeneous chemistry) are imbedded within the meteorological model's



physics package, this component in turn is imbedded within the meteorological model's dynamics package, which also handles chemical tracer advection. A detailed description of the process representation of GEM-MACH, and an evaluation of its performance for pollutants such as ozone and particulate matter (PM) appears in Moran et al. (2013); Makar et al. (2015a, b); Gong et al. (2015); Akingunola et al. (2017).

GEM-MACH is used operationally to issue twice-daily, 48-hour public forecasts of criteria air pollutants (ozone, nitrogen oxides, PM), as well as the the Air Quality Health Index [<https://ec.gc.ca/cas-aqhi/>]. Any improvements to NH_3 in the model may result in better AQHI predictions, since NH_3 is a major precursor of $\text{PM}_{2.5}$, as mentioned in the introduction. We start with a similar, research version of GEM-MACHv2 to make the bidirectional flux modifications. The key differences between this and older versions are the use of a more recent meteorological package (GEMv4.8), the capability to nest in the vertical dimension as well as the horizontal dimension, and improvements to the treatment of fluxes, vertical diffusion, and advection (Akingunola et al. (2017), this issue).

GEM-MACH can be run for many different spatial domains, at various spatial resolutions, and in 2-bin or 12-bin aerosol size distribution modes. For this study we run the model in the 2-bin mode (for computational efficiency), using a nested set of domains. The outer domain at 10-km resolution covering North America, and the inner domain at 2.5-km resolution covering the provinces of Alberta and Saskatchewan. The latter is referred to as the 2.5-km Oil Sands domain. And this set up, along with the emissions described in the next section is hereafter called our "base" simulation.

2.1 Emissions

The emissions used in GEM-MACH (base case) come from Canadian and U.S. emissions inventories: 2011 National Emissions Inventory (NEI) version 1 for U.S. emissions, and the Air Pollutant Emission Inventory (APEI) 2013 for Canadian emissions (2010 for onroad and offroad emissions). Emissions were processed with SMOKE (Sparse Matrix Operator Kernel Emissions, <https://www.cmascenter.org/smoke/>) to convert the inventories into model-ready gridded hourly emissions files for modeling. For more details about these emissions, see Moran et al. (2015) and (Zhang et al., 2017, this issue).

The emissions data for NH_3 from oil sands sources are reported to the Canadian National Pollutant Release Inventory (NPRI) on a "total annual emissions per facility" basis. However, we found an issue with NH_3 in this inventory, which we describe below.

If stack parameters (e.g., stack height and diameter, volume flow rates, temperatures, etc.) are included as part of that data, then the emissions are allocated to large stacks in our configuration of the SMOKE emissions processing system. In the absence of this information, SMOKE will assign default stack parameters based on its source category code. For the Syncrude Canada Ltd. - Mildred Lake Plant Site, NPRI ID 2274, the default stack parameters were: 18.90 m for the stack height (which is within the first model layer), 0.24 m for the stack diameter, 320.0 K for the exhaust temperature, and 0.58 m/s for the exhaust velocity. However, when these defaults were applied in initial



model simulations, they were found to result in erroneous short term plume events with simulated surface NH_3 levels up to 2 orders of magnitude higher than ground observations (Wentworth et al., 2017), and modelled concentrations aloft too low compared to aircraft measurements (see Section 3). Conversely, for species such as SO_2 , for which stack parameters were reported, the model was able to correctly place the SO_2 enhancements in space and time, relative to observations. When the stack parameters of the main stack for this facility were used for NH_3 emissions as well (stack height=183 m, stack diameter=7.9 m, exit temperature=513 K, exit velocity=23.9 m/s, from the NPRI website), the simulation of surface NH_3 was greatly improved. All subsequent simulations reported here make use of this correction.

2.2 Ammonia bidirectional flux parameterization

The bidirectional flux scheme of Zhang et al. (2010) was applied within the GEM-MACHv2 model, replacing the original deposition velocity for NH_3 only (deposition velocity of other gas species follows a scheme based on a multiple resistance approach and a single-layer "big leaf" approach (Wesely, 1989; Zhang et al., 2002; Robichaud and Lin, 1991; Robichaud, 1994)). The bidirectional flux scheme is described in detail in Zhang et al. (2010), but we summarize it here.

Bidirectional exchange occurs between air-soil and air-stomata interfaces. The bidirectional flux (F_t) equation is:

$$F_t = -\frac{C_a - C_c}{R_a + R_b} \quad (1)$$

where R_a and R_b are the aerodynamic and quasi-laminar resistances, respectively. C_a is the NH_3 concentration in the air, and C_c is the canopy compensation point concentration, given by Eq. (2).

$$C_c = \frac{\frac{C_a}{R_a + R_b} + \frac{C_{st}}{R_{st}} + \frac{C_g}{R_{ac} + R_g}}{(R_a + R_b)^{-1} + (R_{st})^{-1} + (R_{ac} + R_g)^{-1} + (R_{cut})^{-1}} \quad (2)$$

where C_{st} and C_g are the stomatal and ground compensation points, and R_i are the resistances in s/m of the ground/soil (R_g), stomata (R_{st}), cuticle (R_{cut}), and in-canopy aerodynamic (R_{ac}). All resistance formulas can be found in Zhang et al. (2003).

Stomata (st) and ground (g) compensation points are both calculated using Eq. (3):

$$C_{st,g} = \frac{A}{T_{st,g}} \exp\left(\frac{-B}{T_{st,g}}\right) \Gamma_{st,g} \quad (3)$$

A and B are constants derived from the equilibria constants for $\text{NH}_3(\text{g})$ in leaves' stomatal cavities to NH_4^+ and OH^- in the water contained in the apoplast within the leaf and in the soil where $\text{NH}_3(\text{g})$ in the soil pore air space is in equilibrium with the NH_4^+ and OH^- dissolved in soil water (Pleim et al., 2013). $A=161500$ mol K/L (Nemitz et al., 2000), or 2.7457×10^{15} ugK/m³ (Pleim et al., 2013) for NH_3 for both stomata and soil. $B=10380$ (Nemitz et al., 2000). $\Gamma_{st,g}$ is the emission potential of the stomata and ground, respectively and, in theory, is equal to the NH_4^+ concentration over the H^+



160 concentration in the apoplast water of the canopy leaves or soil water:

$$\Gamma_{st,g} = \frac{[NH_4^+]_{st,g}}{[H^+]_{st,g}} \quad (4)$$

However, since there are no modeled NH_4^+ and H^+ apoplast water concentrations to use, we use $\Gamma_{st,g}$ in Wen et al. (2014), which are based on long-term empirical averages. Wen et al. (2014) gives a range of values for emission potentials for 26 land use categories (LUCs), and we use the low-end
165 of the values in our model with the following exceptions: We further lower the Γ_g for agriculture LUCs to 800, and increase Γ_{st} of boreal forest LUCs to 3000, all of which were necessary in order to achieve realistic NH_3 concentrations, while staying consistent with findings from the literature.

This version of the model, which we call GEM-MACH-Bidi (or just “bidi” hereafter) was quite sensitive to the selection of emission potentials, which are themselves highly uncertain (Wen et al.,
170 2014). GEM-MACH-Bidi uses the exact same emissions as in the base case, described in the previous section. However, when the sign of F_t in Eq. (1) becomes positive (that is, when $C_a < C_c$), the bidirectional flux acts effectively as an additional source of NH_3 gas, releasing stored NH_3 until and unless the ambient concentration rises to the compensation point concentration. When the flux is negative, net deposition of NH_3 occurs.

175 Other chemical transport models, such as GEOS-Chem and CMAQ use a similar method as Zhang et al. (2010), however, instead of the constant average soil emission potentials used here, they utilize a CMAQ-agroecosystem coupled simulation to calculate a soil pool from which to estimate Γ_g (Bash et al., 2013; Pleim et al., 2013; Zhu et al., 2015). In this case, the emission potential will vary and can go to zero if the NH_4^+ in the pool is depleted. However, it was shown in Wen et al.
180 (2014) that their $\Gamma_{st,g}$ worked well during the same time of year as this investigation (August and September). This time of year was also shown in Zhu et al. (2015) to not have a large effect on emissions from the NH_4^+ pool. Our investigation also has a short time scale of about a month, thus it is expected that the the soil pool would not be depleted over this time period. Finally, given that GEM-MACH is used for real-time air quality forecasts at Environment and Climate Change Canada,
185 it is not desirable for our bidirectional flux scheme to have to rely in advance on another model’s output. Therefore, we use this simplified version, and assess whether its results provide a good enough improvement to simulated NH_3 for less cost in run time.

2.3 Addition of forest fire emissions

Our third model scenario (called “fire+bidi” hereafter) uses the GEM-MACH-Bidi model, and the
190 exact same area emissions and anthropogenic major point emissions as the base and bidi scenarios. However, in addition, we add hourly North American forest fire emissions for all species to the major point emissions. The forest fire emissions system for GEM-MACH (called “Firework”) is described in detail in Pavlovic et al. (2016). Briefly, to calculate the fire emissions for input to FireWork, biomass burning areas are first identified in near real time by the Canadian



195 Wildland Fire Information System (CWFIS), which is operated by the Canadian Forest Service
(<http://cwfis.cfs.nrcan.gc.ca/home>). CWFIS uses fire hotspots detected by NASA's Moderate Resolu-
tion Imaging Spectroradiometer (MODIS) and NOAA's Advanced Very High Resolution Radiometer
(NOAA/AVHRR) and Visible Infrared Imaging Radiometer Suite (VIIRS) imagery as inputs. Daily
total emissions per hotspot are then estimated by the Fire Emission Production Simulator (FEPS)
200 module of the BlueSky Modeling Framework (Larkin et al., 2009). SMOKE was then used to pre-
pare model-ready hourly emissions of several species (including NH_3) in a point-source format for
model input.

In Environment and Climate Change Canada's operational forest fire forecasts, these emissions are
used at 10-km resolution for the domain encompassing North America, with forest fires being treated
205 as point sources with specific plume rise (Pavlovic et al., 2016). We have added 2013 forest fire
emissions which were originally created for the 2013 Firework forecasts to the anthropogenic point
source emissions used in the base case simulation, and modified the GEM-MACH model to be able
to accommodate the changing number of major point sources each day (as the fires are parametrized
as major points, and their number changes daily). Fire plume rise is an ongoing area of investigation
210 (e.g., Heilman et al., 2014; Paugam et al., 2016); smoldering emissions tend to be emitted directly at
the surface, whereas flaming emissions can inject plumes to the upper troposphere. Here, we have set
all fire emissions to be distributed evenly throughout the boundary layer, which is a simplification,
but one that averages out smoldering and flaming plume heights. Different parameterizations of
fire plume rise are currently under development in GEM-MACH. The Fireworks fire emissions are
215 described in detail in Zhang et al., (2017, this issue), and this study represents the first time they have
been used at a 2.5-km horizontal resolution.

2.4 Model setup for three scenarios

The base, bidi, and fire+bidi models were all run with the following input files: Analysis files, which
are the products of meteorological data assimilation and provide optimized initial conditions for
220 the 12 UTC hour of each day, were obtained from ECCO archives (Buehner et al., 2013, 2015;
Caron et al., 2015), and the numerical weather prediction regional GEM model was run regionally
at 10-km and the high resolution GEM model was run at 2.5-km resolution to produce meteorological
files to drive the model simulation. The base, bidi, and fire+bidi scenarios were run from 1 August to
7 September, 2013, where the first 11 days were "spin up" in order to allow chemical concentrations
225 to stabilize, and are not used in our evaluation. This is a sufficient amount of spinup time, given that
the atmospheric lifetime of NH_3 is typically up to 1 day (Seinfeld and Pandis, 1998; Aneja et al.,
2001), and given that it is close to the transport time of air crossing the larger North American
domain. The time period of 12 August to 7 September was chosen to coincide with the intensive
measurement campaign described in Section 3.



230 The model was run in a nested setup, whereby the North American domain was run at 10-km resolution using “climatological” chemical initial and boundary conditions from a 1-year MOZART simulation for all pollutants (Giordano et al., 2015). The nested Oil Sands region (which covers most of Alberta and Saskatchewan) was run at 2.5-km horizontal resolution, using the initial and boundary conditions from the 10-km North American model run. Figure 1 shows the two model domains.

235 The model simulations for the pilot and nested domains were not run as a continuous multiday forecast, but rather following to the operational air quality forecast process, where the meteorological values are updated regularly with new analyses, in order to prevent chaotic drift of the model meteorology from observations. Consequently, our simulation setup comprises simulations on the North American domain in 30-hour cycles starting at 12 UTC, and the Oil Sands domain in 24-hour
240 cycles starting at 18 UTC (the 6 hour lag being required to allow meteorological spinup of the lower resolution model). The next cycle uses the chemical concentrations from the end of the last cycle as initial conditions for the next 24-30 hours. This system of staggered meteorological driving forecasts with a continuous concentration record continues until the full time period completes.

We run GEM-MACH in the 2-bin particle mode, which means that particles fall in either fine
245 mode (diameter 0-2.5 μm) or coarse mode (diameter 2.5-10 μm), for computational efficiency (although sub-binning is used in some particle microphysics processes in order to ensure an accurate representation of particle microphysics (Moran et al., 2010)), and in order to follow the setup used for the operational 10-km resolution GEM-MACH forecast.

3 Measurements

250 Our three model simulations (base, bidi, and fire+bidi) are evaluated with surface, aircraft, and Cross-track Infrared Sounder (CrIS) satellite measurements. We briefly describe each of these observations below.

3.1 AMS13 ground measurements

An extensive suite of instrumentation was deployed at monitoring site AMS13 (57.1492°N, 111.6422°W,
255 270 m.a.s.l., Fig. 2) from 7 August 2013 until 12 September 2013. Mining operations and bitumen upgrading facilities are 5 km to the south and north of the site. It is surrounded by boreal forest, with dominant winds from the west. NH_3 , fine particulate ammonium and nitrate, and other species were measured by the Ambient Ion Monitor-Ion Chromatograph (AIM-IC), via an inlet 4.55 m off the ground (Wentworth et al., 2017). The uncertainty of these measurements is $\pm 15\%$. These measurements appear in this issue (Wentworth et al., 2017), and are described in more detail there.
260

Data gaps sometimes appeared in the surface NH_3 time series for the following reasons: instrument zero (Aug 14/15 and 17/18), instrument maintenance (Aug 19) and a power outage (Aug 27/28).



3.2 Aircraft measurements

265 During the Oil Sands Monitoring Intensive campaign, there were a total of 22 flights spanning 13
August to 7 September 2013. These measurements are described in detail in Shephard et al. (2015);
Gordon et al. (2015); Liggio et al. (2016); Li et al. (2017), and are summarized here. Aircraft NH_3
measurements were conducted with a dual quantum cascade laser (QCL) trace gas monitor (Aero-
dyne Inc., Billerica, MA, USA; McManus et al., 2008), collecting data every 1 s. Outside air was
270 sampled through a heated Teflon inlet tube shared with a high-resolution time-of-flight chemical
ionization mass spectrometer (HR-ToF-CIMS); the flow rate through the QCL was 10.8 L min^{-1} .
The 1σ uncertainty for each measurement is estimated to be $\pm 0.3 \text{ ppbv}$ ($\pm 35\%$) (Shephard et al.,
2015).

Particulate NH_4^+ and NO_3^- ($0 < 1 \mu\text{m}$ in diameter) were measured by the Aerodyne high-resolution
275 time-of-flight aerosol mass spectrometer (HR-ToF-AMS) instrument on board the same flights,
which collected data every 10 s. The ambient air was drawn through a forward facing, shrouded
isokinetic particle inlet from which the HR-ToF-AMS sub-sampled. The total residence time in the
inlet and associated tubing was approximately 1 second. The error on these measurements is $\pm 9\%$.
(Liggio et al., 2016)

280 Figure 2 shows a sample flight path from the campaign from 13 August 2013 – one of the thirteen
flights with valid NH_3 measurements. The others took place on 15-17, 19 (two this day), 22-24,
26, 28 August, and 5-6 September 2013. NH_3 data on the other nine flights were invalidated due to
instrument issues (those on 14, 20-21, 29, 31 August, and 2-4 September 2013), but were successful
for the NH_4^+ and NO_3^- measurements.

285 3.3 CrIS satellite measurements

CrIS was launched in late October 2011 on board the Suomi NPP platform. CrIS follows a sun-
synchronous orbit with a daytime overpass time at 13:30 (ascending) and a night time equator over-
pass at 1:30 (descending), local time. The instrument scans along a 2200 km swath using a 3×3
array of circular pixels with a diameter of 14 km at nadir for each pixel. The CrIS Fast Physical
290 Retrieval (CFPR) described by Shephard and Cady-Pereira (2015) is used to perform satellite pro-
file retrievals of ammonia volume mixing ratio (VMR) given the infrared emission spectrum from
the atmosphere. This retrieval uses an optimal estimation approach (Rogers, 2000) that provides the
satellite vertical sensitivity (averaging kernels) and an estimate of the total errors (error covariance
matrix).

295 We take the CrIS retrieved profile and match it up with the closest model profile in both distance
and time. Compute the distance between the CrIS pixel and model field for each time step, and
then select the time step that best matches the satellite overpass time. Since the model time steps are
every hour with a 10-km spatial resolution they are always matched up to better than half an hour, and



within 5 km. Figure 3 shows a map with four boxed regions indicating where model-measurement
300 pairs were sampled for this study. These and the corresponding satellite fields will be discussed later
in the model evaluation section below.

4 Model evaluation

An older version of GEM-MACH (v1.5.1) has been compared to TES satellite and aircraft mea-
surements of ammonia over the AOSR (Shephard et al., 2015). Simulations with that version of the
305 model were shown to be biased low, by about -0.5 ppbv, throughout the lower-tropospheric vertical
profile. This represented a substantial deficit in the model predicted sources of NH_3 , prompting the
current work. We now compare our three GEM-MACH simulations (base, bidi, and fire+bidi) against
surface point measurements at the measurement site near an oil sands facility (AMS13), aircraft mea-
surements over the broader AOSR, and satellite measurements over the Alberta and Saskatchewan
310 area. We will discuss which simulation agrees best with measurements and where there may still be
room for additional model improvement.

4.1 At the AMS13 ground site

Figure 4 shows the timeseries of the concentrations of NH_3 and its reaction products, fine-particulate
 NH_4^+ and NO_3^- , as well as its aerosol sink SO_4^{2-} at the AMS13 Oil Sands ground site for the observa-
315 tions and three model simulations. Note that the y-scale is logarithmic to better show the differences
between the three model scenarios and the measurements - however, this means that when concen-
trations drop to zero in the model, the line becomes disjointed. This is mainly evident in the NO_3^-
time series (Fig. 4c). Figure 4 shows that the base model (green) background concentrations of NH_3
are biased low (nearly 0 ppbv when there is no plume influence) compared to the measurements
(orange). Only during the spike on September 3-4th does the base model exceed the measured val-
ues, probably indicating a local plume event fumigating to a lesser extent in the observations than
was assumed in the model. The concentrations of the base case are biased low compared the surface
measurements by a median of -0.35 ppbv over the time period of the campaign – comparable to
the bias observed in satellite observations in Shephard et al. (2015). The model-measurement dif-
325 ferences are shown in Fig. 5a. In Fig. 4, the bidi model (blue line) and fire+bidi model (red line)
show a significant improvement to the NH_3 concentrations during the background times, compared
to the base case model (green line). Unfortunately, during some time periods, these two versions of
the model overestimate NH_3 : During August 13th, the model adds a significant level of NH_3 due
to fire emissions, however the surface *in situ* observations show no evidence of fire impact. During
330 other time periods (e.g., 30 August to 3 September, and 4-7 September), the bidi model appears to
have put too much NH_3 into the system. Therefore, the bidi model bias is now 0.30 ppbv too high



(median), and the fire+bidi bias is 0.32 ppbv high (median) over the time period of the campaign, resulting in an overall improvement of only 0.03 ppbv in the model bias.

When the influence of local plumes (defined as the base model exceeding 0.5 ppbv) is removed
335 from the time series, the median biases are as follows: -0.36 ppbv for the base model, +0.26 ppbv
for the bidi model, and +0.28 ppbv for the fire model – corresponding to an overall improvement of
0.08 ppbv in model bias for background concentrations.

While the bias improvement is small, the bidi and fire+bidi both have greatly improved correlation
coefficients (from $R=0.2$ to 0.4) and slopes much closer to 1 (from 0.035 to 0.614), showing that
340 those added sources are important to improve model results (Fig. 6a). The correlation coefficients
and slopes were similarly improved when the plume influence was removed, and only background-
level concentrations were examined.

While Fig. 4a to 6a show that the addition of bidirectional flux significantly improves the model
correlation coefficient, slope, and bias, there is still room for improvement. While inherent limita-
345 tions from model resolution and uncertainties may be responsible for the remaining bias, it is likely
that (a) the emission potentials for the land use categories (LUCs) in the region may be causing too
much re-emission of NH_3 , and need refinement, and (b) the fire emissions of NH_3 are not properly
distributed in the vertical, placing too much NH_3 near the surface and/or the fire emission factors for
 NH_3 are too high.

Refinement needed for the emission potentials and LUCs may be a significant cause of the bidi
and fire+bidi model biases. Rooney et al. (2012) have shown that about 64% of the AOSR are wet-
lands (fens, bogs and marshes), which *should* be mapped to the swamp LUC. However, our model
currently assigns the AOSR landscape to evergreen needleleaf trees, deciduous broadleaf trees, in-
land lake, mixed shrubs, and mixed forests (and none of the region to swamp). This would lead to an
355 overestimation of re-emission given that bogs are fairly acidic and our swamp emission potential is
lower than the aforementioned LUCs. Other evidence for these two explanations will be presented
below in Section 4.3.

The time series, model-vs-measured correlations, and model biases of NH_4^+ , NO_3^- , and SO_4^{2-}
are also shown in Fig. 4 to 6 (b, c, and d, respectively). For NH_4^+ and SO_4^{2-} there is very little
360 change despite the increase in NH_3 that the bidirectional flux yields. The bias is very small for all
three model scenarios, and the correlation coefficients are all relatively poor. So while there is an
improvement to modelled NH_3 with bidirectional flux, there is a neutral affect on fine particulate
 NH_4^+ . This may be because the charge of NH_4^+ in the particles is already enough in the base model
to balance the charge of $2 \times \text{SO}_4^{2-} + \text{NO}_3^-$ in the aerosols, thus, causing any additional NH_3 (from
365 bidi and fires) to remain in the gas phase. Or it could be due to additional wet scavenging of the
additional ammonium, which will be discussed in Section 5.2. The change in NH_3 concentrations
has no effect on SO_4^{2-} since particulate SO_4^{2-} is not sensitive to the amount of $\text{NH}_3/\text{NH}_4^+$ available,
and is dominated by anthropogenic emissions. For NO_3^- , the base model bias was quite small at 0.01



$\mu\text{m}/\text{m}^3$, however the addition of bidi and fire+bidi further reduced that bias to 0.0011 and 0.0004 $\mu\text{m}/\text{m}^3$, respectively, which is a significant improvement. The correlation coefficient for NO_3^- also improved from about 0.1 to 0.3 (Fig. 6c).

4.2 Along the OS campaign flight paths

There were 13 flights during the OS campaign that had valid (above detection limit, and no instrument error) NH_3 measurements, and 22 flights that had valid NH_4^+ (0-1 μm diameter) measurements. The flight path of the first flight, which occurred on 13 August 2013 is shown in Fig. 2 as an example.

Figure 7 shows the NH_3 concentrations along this flight path over time. Here the hourly model output is interpolated to the same time frequency as the measurements. The model also has spatial resolution limits when comparing to the aircraft. However, we clearly see that for this flight, the bidirectional flux has increased NH_3 concentrations, bringing them closer to the measured values. Figure 8 shows the corresponding model-measurement difference and the model vs measurement scatter plots for the combined set of all flight paths for hourly-average concentrations of NH_3 and NH_4^+ . For NH_3 the median base model bias is -0.75 ppbv, comparable to the bias observed in Shephard et al., 2015, with the bidi model bias improving to -0.24 ppbv, and the fire+bidi bias to -0.23 ppbv. Also the best correlation coefficient and slope is achieved by the fire+bidi scenario. The use of the bidirectional flux has thus reduced the model bias relative to the aircraft observations by a factor of three.

Again, the NH_4^+ results show little change despite the increase in NH_3 concentrations. The small bias from the base case gets insignificantly smaller, and the slope and correlation coefficients are all negligibly changed.

4.3 In the vertical profiles across the region

The CrIS satellite has many observations over North America during the 2013 Oil Sands campaign. We have evaluated the model with these observations in a number of ways:

1. Daytime overall average in this area from Aug 12 - September 7th, 2013 comparisons over a large region encompassing Alberta and Saskatchewan (blue box in Fig. 3, latitude range: 48-60 °N, longitude range: 100-122 °W), which contains agricultural areas, a number of cities, the northern boreal forest, and the Oil Sands facilities.
2. Case studies where we attempt to isolate fire emissions (magenta box in Fig. 3), and non-fire conditions (cyan and black boxes in Fig. 3) to evaluate both new components (fires and bidi) of the model.

The latitude and longitude ranges of our model-measurement pairs are given in Table 1. The satellite passes over these regions at approximately 1pm and 1am local time.



In the large box spanning northern Alberta and Saskatchewan, there were over 60 000 model-measurement pairs between the model and the CrIS satellite during August 12th to September 7th, 2013. Figure 3 shows the surface NH_3 concentrations over that region on three sample days (3 Sept, 405 1 Sept and 12 Aug, 2013), as well as sample Aqua MODIS true colour composite map for that day. Figure 9 presents statistics for the entire dataset in a box and whiskers plot of the vertical NH_3 profiles at five vertical levels, along with the model–satellite bias for the base model, bidi model, and fire+bidi model. The right-most panel shows the diagonal elements of the CrIS averaging kernels, illustrating the sensitivity of the satellite measurements to each vertical level.

410 In Fig. 9 we see that the fire+bidi model has the smallest bias in the highest three layers, but the bidi model has the smallest bias in the two lowest layers, whereas the fire+bidi model increases NH_3 concentrations further (though still a smaller absolute bias compared to the base case). This could be due to an overestimate of the bidirectional flux re-emissions or of the fire emissions, or to an underestimate of the altitude of the fire emissions, or a combination of all three factors. In order to 415 distinguish between these possibilities, two case studies were examined further below.

4.3.1 Case study 1: clear-sky days with little fire influence - evaluating bidi

In order to evaluate the bidirectional flux component separately from the fire component, we selected September 1st (southern, agricultural region - black box in Fig. 3b), and 3rd (northern, boreal forest and AOSR region - cyan box in Fig. 3a), where the MODIS map (EOSDIS NASA World view 420 map, worldview.earthdata.nasa.gov) shows very little hot spots from fires, and that the conditions were relatively cloud and smoke free (which yield the most CrIS observations). See Table 1 for the latitude and longitude ranges. Figure 3 also shows the surface NH_3 concentrations as observed by CrIS on each of those days. Figure 10a shows that in the north, the bidi model improves the bias from -0.84 ppbv to -0.07 ppbv in the lowest vertical level, and smaller, but still significant, improvements 425 to the bias at the other levels. The fire+bidi model has a nearly identical impact as the bidi model, which is expected in a fire-free zone. Therefore, the GEM-MACH-Bidi model performs very well in northern Alberta and Saskatchewan where there is mainly boreal forest, and background-level NH_3 concentrations. This also implies that the LUC assignment discussed in Section 4.1 may only apply to a small region around the AOSR, and not to the overall large region we've defined here.

430 In the southern region (Fig. 10b), the addition of bidirectional flux moves the bias from near-zero to +1.02 ppbv. In this case, the base model with no bidirectional flux appears to be the most accurate model in areas dominated by agricultural sources. There are two possible explanations: a) agricultural emissions are too high in the base model, and the addition of the bidirectional flux leads to an overestimation of the NH_3 amounts, or b) re-emissions from bidirectional flux from crops are not significant. The literature (Bash et al., 2010; Massad et al., 2010; Zhang et al., 2010; Zhu et al., 2015) 435 indicate that crops do indeed re-emit NH_3 , therefore, (a) is the more likely explanation. The agriculture NH_3 emission inventory we used was created by the NAESI (National Agri-Environmental



Standards Initiative) project (Bittman et al., 2008; Ayres et al., 2009; Makar et al., 2009) have about 30-200% uncertainty associated with them (Bouwman et al., 1997; Asman et al., 1998). Therefore, 440 with improved national NH₃ emission inventories, the GEM-MACH-Bidi should improve model results across the domain.

4.3.2 Case study 2: a clear day with significant fire influence - evaluating fires

In order to evaluate the fire component separately from the bidirectional flux, we selected August 12th (a northern region with little-to-no agricultural contributions) where the MODIS map shows 445 numerous hot spots from fires and smokey conditions (Fig. 3c, magenta box). The base and bidi models underestimate NH₃ concentrations (Fig. 10c) by -6.22 and -5.84 ppbv, respectively (in the lowest vertical layer), but that the fire+bidi model overestimates NH₃ by +4.06 ppbv. The fire+bidi version of the model still has the lowest bias of the three simulations, however, either (a) the fire+bidi model does not distribute the fire emissions properly in the vertical, (b) the fire emissions of NH₃ 450 are too high, and/or (c) the model is not properly representing NO₂ and SO₂ in the fire, and so the conversion of NH₃ to NH₄⁺ is underestimated. Both fire plume rise and fire emission factors are on-going areas of study. It is likely a combination of all three explanations; in the model the fire emissions are distributed evenly through out the boundary layer (the first 3-4 layers from Fig. 10c, however, Shinozuka et al. (2011) suggest that sometimes the fire plumes are in a Gaussian 455 distribution located in a thin layer aloft (which is an option for GEM-MACH that is currently under development). However, should that be the case, the bias would move negative at at least one of the levels in Fig. 10c, which it does not (unless the fire plume is actually above 4 km, however, it was found that the plume heights for the Fort McMurray fires of 2016 reached only up to 3-3.5 km, shown by the lidar on CALIPSO satellite). Figure 10c shows that the positive bias extends throughout the 460 first three vertical layers, and in the top two vertical layers, the bias does not move further negative (as would happen in the fire plume were actually at those altitudes in real life). Explanation (b) seems likely, as the uncertainty on emission factors for NH₃ from wildfires is very large (e.g., 50-100% depending on the fuel type Urbanski, 2014), and could easily be overestimated. Similarly, the NO_x and SO₂ emission factors have uncertainties of 10-40% (Urbanski, 2014).

465 Unfortunately, there were no flights that captured the fine structure of the fire plumes during the 2013 monitoring intensive campaign that can be used to further corroborate the vertical distribution of the fire plumes. There will however be flight observations of fires during the planned 2018 AOSR measurement campaign. Therefore, the model may be further improved with reduced NH₃ emission factors for fires, and/or improved vertical distribution of fire plumes.



470 5 Impacts of bidirectional flux and forest fires on NH₃ concentrations

5.1 Effect on ambient concentrations

Given that the overall fire+bidi model agrees best with measurements in the greater Alberta/Saskatchewan region (discussed throughout Section 4) and contains all known missing sources of NH₃, we can use the model to answer one of our key questions: What percent contributions to total ambient NH₃ concentrations came from bidirectional flux and from forest fires during the study time period? We do so by subtracting the bidi model output from the fire+bidi model output to get the forest fire component, and subtracting the base model output from the bidi model output to get the bidi component. The absolute differences are calculated as follows:

$$bidicomponent = NH_3^{bidi} - NH_3^{base} \quad (5)$$

480

$$firecomponent = NH_3^{fire+bidi} - NH_3^{bidi}, \quad (6)$$

which tell us how many ppbv of NH₃ on average comes from re-emissions of NH₃ (upward component of bidirectional flux), and from fire emissions.

The percent differences are calculated as follows:

$$485 \quad bidipercents = \frac{NH_3^{bidi} - NH_3^{base}}{NH_3^{fire+bidi}} \times 100\% \quad (7)$$

$$firepercent = \frac{NH_3^{fire+bidi} - NH_3^{bidi}}{NH_3^{fire+bidi}} \times 100\%, \quad (8)$$

which tell us what percent of *total* NH₃ concentrations on average comes from re-emissions of NH₃ (upward component of bidirectional flux), and from fire emissions, assuming the NH₃ from our fire+bidi simulation is the true total NH₃.

Over the 2.5-km model domain (averaged over 12 August to 7 September 2013), we do this calculation (See Fig. 11) and get an average of 20.3% (or 0.42 ppbv) of ambient surface NH₃ concentrations comes from forest fires – though the median amount is only 10.4% for fires. The mean and median are so different because fires are sporadic large contributions to NH₃ concentrations, and the mean value is more sensitive to the big outliers. We get an average of 56.6% (or 1.24 ppbv) from bidirectional flux (56.3% median). The remaining 23.1% (average) 33.3 % (median) comes from direct emissions from anthropogenic sources (agriculture, fossil fuel combustion, oil sands industry, etc). These numbers are summarized in Table 2.

Over the model domain, the minimum bidi influence on surface NH₃ is just north of Edmonton, where only 1% of NH₃ comes from bidi. Similarly, two AOSR facilities north of Fort McMurray stand out as having small bidi influence (12-40 %, surrounded by values in the 90s% - Fig. 11, d). Also, any remote region with fire emissions will have a small percentage contribution from bidirectional flux during the fires, as they are in northern Saskatchewan (Fig. 11,d). This is expected



given that the average concentrations in cities and near large sources are very close to, or exceed
505 the compensation point. The absolute maximum in the bidi component map is 4.5 ppbv in the lower
right corner (an agricultural region with high NH_3 emissions), and the minimum is 0 ppbv (Fig.
11,b). This means that nowhere in the domain, did the bidirectional flux formula result in *more* net
deposition than the base model calculated via the Welesley/Robichaud scheme. The maximum fire
contribution is 27.9 ppbv where large fires occurred in northern Saskatchewan (Fig. 11, c).

510 5.2 Effect on Deposition

Similar to our analysis from the previous section, we can use the model to determine how bidirec-
tional flux and fires impact daily NH_3 dry deposition. Figure 12 shows the average daily net dry
deposition (or net flux) of NH_3 from the base, bidi, and fire+bidi models. Negative (or blue) indi-
cates net deposition (downward flux), and positive (or red), net emission (upward flux). The base
515 model (Fig. 12a) had no re-emission (upward flux) option, thus NH_3 was always net deposited in
that scenario, and was 9.85×10^{-6} moles/ m^2 /day on average. The bidi (Fig. 12b) and fire+bidi (Fig.
12c) maps show that over much of the Alberta and Saskatchewan area, there is net emission of NH_3 ,
and net deposition only occurs where concentrations are highest (near the cities, agriculture, and for-
est fires). Average flux has changed to net positive over the domain, with averages of $+2.44 \times 10^{-5}$
520 moles/ m^2 /day and $+2.10 \times 10^{-5}$ moles/ m^2 /day for the bidi and fire+bidi cases, respectively. Note that
this result is partly due to our assumption of an infinite soil pool of NH_4^+ . Following the soil pool
approach (Pleim et al., 2013; Zhu et al., 2015), the soil pool of NH_4^+ would eventually get depleted,
thus the average net flux may not be as largely positive as we calculated in this study.

In the AOSR near Fort McMurray, we can compare our NH_3 dry deposition results to those
525 calculated in Hsu and Clair (2015). Their values range from 0.7 to 1.25 kg-N/ha/year (or 1.13 to
 2.01×10^{-5} mol/ m^2 /day), and ours are 10× lower at around 0.13 kg-N/ha/year (or 2.12×10^{-6}
mol/ m^2 /day) near Fort McMurray, and do not vary much among our three model scenarios. Our
deposition underestimate may be partially due to the fact that our modelled ambient NH_3 concentra-
tions are also low compared to those measured in Hsu and Clair (2016) near Fort McMurray. They
530 measured an average of 1.55 ± 0.6 ppbv ($1.9 \mu\text{g}/\text{m}^3$) at Fort McMurray, whereas our fire+bidi model
has an average of 1.01 ppbv there (0.73 ppbv in bidi, and 0.39 in base).

Figure 13 (a) shows the difference in deposition between the bidi and base cases – essentially
the contribution of bidi to the total flux. The bidi model has increased flux in the positive direction
everywhere by an average of $+3.43 \times 10^{-5}$ $\mu\text{moles}/\text{m}^2$ across the domain. Figure 13 (b) shows the
535 difference in deposition between the fire+bidi and bidi cases - which is the contribution of fires to
the total flux. The fires have decreased flux (in other words increased downward flux, or deposition)
over large swaths of the domain. The fires contributed an average of -3.47×10^{-6} $\mu\text{moles}/\text{m}^2$ of
deposition across the domain.



The wet deposition of NH_4^+ was also modelled and analysed in a similar way (Fig. 14). Unlike NH_3 , since there is no re-emissions of NH_4^+ in the model, all flux is negative. While the particulate NH_4^+ concentrations did not change much in our three simulations (see Sections 4.1 and 4.2), the wet deposition of NH_4^+ increased significantly going from the base to bidi to fire+bidi models (Fig. 14 from a to b to c). It would seem that the increased NH_3 concentrations were scavenged by precipitation. The average NH_4^+ deposition from the three simulations was: $-2.04 \times 10^{-5} \mu\text{moles/m}^2$ for base, $-4.25 \times 10^{-5} \mu\text{moles/m}^2$ for bidi, and $-5.86 \times 10^{-5} \mu\text{moles/m}^2$ for fire+bidi. That is nearly a threefold increase in the NH_4^+ deposition due to the increased NH_3 concentrations that the fire+bidi simulation yields. Note that in the soil pool approach of Pleim et al. (2013); Zhu et al. (2015), this deposited NH_4^+ would contribute towards the soil pool, which could be re-emitted as NH_3 . In our case, once deposited, the NH_4^+ is not re-emitted.

In the three scenarios, the average daily relative ratio of dry/wet deposition was: 0.43 for base, -0.77 for bidi, and -0.51 for fire+bidi. Since all average ratios are less than 1, this means that most of the removal process is from wet deposition, rather than dry deposition (even for the base case that had no re-emission of NH_3). Therefore, increased monitoring of wet deposition in the region would be useful. These results may also be useful for AEP terrestrial/aquatic scientists interested in nitrogen eutrophication. The negative value for the bidi and fire+bidi cases are because of the average upward direction of NH_3 . Maps of these ratios can be found in the supplemental material.

6 Conclusions

The GEM-MACHv2 air quality forecasting model was altered to include both the Zhang et al. (2010) bidirectional flux scheme for NH_3 and forest fire emissions of all species. This “fire+bidi” model greatly improves the simulated NH_3 in the modelled Oil Sands domain at 2.5-km resolution when compared to independent *in situ* measurements at the ground (at the AMS13 oil sands monitoring site) and aloft (aircraft measurements), as well as at 10-km resolution when compared to remote sensing from the CrIS instrument. We have also shown that for further improvements in the Alberta/Saskatchewan region, the NH_3 emission factors for fires, and the NH_3 emissions from agriculture likely need to be reduced. This suggests that the fire+bidi model shows promise for improving NH_3 model predictions elsewhere and during other time periods. However, more work is required to validate the model in other regions of the continent (e.g., with the Wood Buffalo Environmental Association (WBEA) and the U.S. Ammonia Monitoring Network (AMoN) surface networks, and further CrIS satellite measurements), and for different time periods (e.g., springtime fertilizer season). We’ve also shown that for further improvements in the Alberta/Saskatchewan region, the NH_3 emission factors for fires, and the NH_3 emissions from agriculture likely need to be reduced.

Despite the significant increase in NH_3 concentrations with these additional sources, the impact on its byproduct, NH_4^+ was miniscule - as was the change to SO_4^{2-} concentrations. The model bias



for those species was not significantly changed in either direction. This is probably because of the
575 extra NH_4^+ wet scavenging by precipitation, and the NH_3 concentrations were already high enough
(before adding the extra sources) to charge balance the SO_4^{2-} and NO_3^- in the aerosols. Thus, any
additional NH_3 would remain in the gas phase. That said, the model bias for NO_3^- was essentially
removed with the fire+bidi model.

By running the base, bidi, and fire+bidi model scenarios, and taking the fire+bidi results as
580 "true", we were able to calculate their differences and determine the average contributions from
each source. We found that, on average, during the 12 August to 7 September 2013 time period in
the Alberta/Saskatchewan model domain, 23.1% of surface NH_3 comes from anthropogenic sources,
56.6% of surface NH_3 comes from bidirectional flux (re-emission from soils and plants), and 20.3%
of NH_3 comes from forest fires. Possible sources of error that remain in the bidi and fire+bidi simu-
585 lations are the agricultural and fire emissions of NH_3 , as well as the emission potentials for different
land-use categories. The fraction of NH_3 from fires is highly variable depending on the time periods
and spatial domain analysed: on average from 12 August to 7 September 2013, the largest impact
was in northern Saskatchewan. The bidirectional flux process has decreased NH_3 deposition on av-
erage, resulting in a net emission of NH_3 across the domain. This increase due to the bidirectional
590 flux, coupled with the increase driven by fires, enhances wet deposition of NH_4^+ by a factor of three.

Acknowledgements. The project was supported by Environment and Climate Change Canada's Oil Sands Mon-
itoring program (OSM), and the Climate Change and Air Quality Program (CCAP). We would also like to
acknowledge the University of Wisconsin-Madison Space Science and Engineering Center Atmosphere SIPS
team sponsored under NASA contract NNG15HZ38C for providing us with the CrIS level 1 and 2 input data,
595 in particular Keven Hrpeck and Liam Gumley



References

- Akingunola, A., Makar, P. A., Moran, M., Zhang, J., and Zheng, Q.: Atmos. Chem. Phys., 2017.
- Aneja, V., Bunton, B., Walker, J., and Malik, B.: Measurement and analysis of atmospheric ammonia emissions from anaerobic lagoons, Atmos. Environ., 35, 1949 – 1958, doi:[https://doi.org/10.1016/S1352-2310\(00\)00547-1](https://doi.org/10.1016/S1352-2310(00)00547-1), 2001.
- 600 Asman, W. A. H., Sutton, M. A., and Schjorring, J. K.: Ammonia: emission, atmospheric transport and deposition, New Phytologist, 139, 27–48, doi:[10.1046/j.1469-8137.1998.00180.x](https://doi.org/10.1046/j.1469-8137.1998.00180.x), 1998.
- Ayres, J., Bittman, S., Girdhar, S., Sheppard, S., Niemi, D., Ratte, D., and Smith, P.: Chapter 5: Sources of Ammonia Emissions, in: The 2008 Canadian Atmospheric Assessment of Agricultural Ammonia, Environment and Climate Change Canada, Gatineau, QC, Canada, 2009.
- 605 Bash, J. O., Walker, J. T., Katul, G. G., Jones, M. R., Nemitz, E., and Robarge, W. P.: Estimation of In-Canopy Ammonia sources and sinks in a fertilized Zea mays field, Environ. Sci. Tech., 44, 1683–1689, doi:[10.1021/es9037269](https://doi.org/10.1021/es9037269), 2010.
- Bash, J. O., Cooter, E. J., Dennis, R. L., Walker, J. T., and Pleim, J. E.: Evaluation of a regional air-quality model with bidirectional NH₃ exchange coupled to an agroecosystem model, Biogeosciences, 10, 1635–1645, doi:[10.5194/bg-10-1635-2013](https://doi.org/10.5194/bg-10-1635-2013), 2013.
- 610 Beer, R., Sheppard, M. W., Kulawik, S. S., Clough, S. A., Eldering, A., Bowman, K. W., Sander, S. P., Fisher, B. M., Payne, V. H., Luo, M., Osterman, G. B., and Worden, J. R.: First satellite observations of lower tropospheric ammonia and methanol, Geophys. Res. Lett., 35, doi:[10.1029/2008GL033642](https://doi.org/10.1029/2008GL033642), I09801, 2008.
- 615 Behera, S. N., Sharma, M., Aneja, V. P., and Balasubramanian, R.: Ammonia in the atmosphere: a review on emission sources, atmospheric chemistry and deposition on terrestrial bodies, Environ. Sci. Pollut. Res. Int., 20, 8092–8131, doi:[10.1007/s11356-013-2051-9](https://doi.org/10.1007/s11356-013-2051-9), 2013.
- Bittman, S., Ayres, J., S. Sheppard, S., and Girdhar, S.: Chapter 4: Emission Inventory Development, in: The 2008 Canadian Atmospheric Assessment of Agricultural Ammonia, Environment and Climate Change Canada, Gatineau, QC, Canada, 2008.
- 620 Bouwman, A., Lee, D. S., Asman, W. A. H., Dentener, F. J., van der Hoek, K. W., and Olivier, J. G. J.: A global high-resolution emission inventory for ammonia, Glob. Biogeochem. Cycles, 11, 561–587, doi:[10.1029/97GB02266](https://doi.org/10.1029/97GB02266), 1997.
- Buehner, M., Morneau, J., and Charette, C.: Four-dimensional ensemble-variational data assimilation for global deterministic weather prediction, Nonlinear Processes Geophys., 20, 669–682, doi:[10.5194/npg-20-669-2013](https://doi.org/10.5194/npg-20-669-2013), 2013.
- 625 Buehner, M., McTaggart-Cowan, R., Beaulne, A., Charette, C., Garand, L., Heilliette, S., Lapalme, E., Laroche, S. S. R. M., Morneau, J., and Zadra, A.: Implementation of Deterministic Weather Forecasting Systems based on Ensemble-Variational Data Assimilation at Environment Canada. Part I: The Global System, Mon. Wea. Rev., 143, 2532–2559, doi:[10.1175/MWR-D-14-00354.1](https://doi.org/10.1175/MWR-D-14-00354.1), 2015.
- 630 Bytnerowicz, A., Fraczek, W., Schilling, S., and Alexander, D.: Spatial and temporal distribution of ambient nitric acid and ammonia in the Athabasca Oil Sands Region, Alberta, J. Limnol., 69, 11–21, doi:[10.3274/JL10-69-S1-03](https://doi.org/10.3274/JL10-69-S1-03), 2010.



- 635 Carfrae, J. A., Sheppard, L. J., Raven, J., Stein, W., Leith, I. D., Theobald, A., and Crossley, A.: Early effects of atmospheric ammonia deposition on *Calluna vulgaris* (L.) hull growing on anombrotrophic peat bog, *Water Air Soil Pollut. Focus*, 4, 229–239, doi:10.1007/s11267-004-3033-1, 2004.
- Caron, J.-F., Milewski, T., Buehner, M., Fillion, L., Reszka, M., Macpherson, S., and St-James, J.: Implementation of deterministic weather forecasting systems based on ensemble–variational data assimilation at Environment Canada. Part II: The regional system, *Mon. Wea. Rev.*, 143, 2560–2580, doi:10.1175/MWR-D-14-00353.1, 2015.
- 640 Charpentier, A. D., Bergerson, J. A., and McLean, H. L.: Understanding the Canadian oil sands industry’s greenhouse gas emissions, *Environ. Res. Lett.*, 4, 1–11, doi:10.1088/1748-9326/4/1/014005, 2009.
- Ciais, P., Sabine, C., Bala, G., Bopp, L., Brovkin, V., Canadell, J., Chhabra, A., DeFries, R., Galloway, J., Heimann, M., Jones, C., Le Quéré, C., Myneni, R. B., Piao, S., and Thornton, P.: Carbon and Other Biogeochemical Cycles, in: *Climate Change 2013: The Physical Science Basis, Contribution of Working Group I to the Fifth Assessment Report of the Intergovernmental Panel on Climate Change*, edited by Stocker, T. F., Qin, D., Plattner, G.-K., Tignor, M., Allen, S. K., Boschung, J., Nauels, A., Xia, Y., Bex, V., and Midgley, P. M., p. 465–570, Cambridge University Press, Cambridge, United Kingdom and New York, NY, USA, 2013.
- 650 Clarisse, L., Clerbaux, C., Dentener, F., Hurtmans, D., and Coheur, P.-F.: Global ammonia distribution derived from infrared satellite observations, *Nature Geosci.*, 2, doi:10.1038/ngeo551, 109801, 2009.
- Dragosits, U., Theobald, M., Place, C., Lord, E., Webb, J., Hill, J., ApSimon, H., and Sutton, M.: Ammonia emission, deposition and impact assessment at the field scale: a case study of sub-grid spatial variability, *Environmental Pollution*, 117, 147 – 158, doi:https://doi.org/10.1016/S0269-7491(01)00147-6, 2002.
- 655 Ellis, R., Murphy, J. G., Markovic, M. Z., VandenBoer, T. C., Makar, P. A., Brooks, J., and Mihele, C.: The influence of gas-particle partitioning and surface-atmosphere exchange on ammonia during BAQS-Met, *Atmos. Chem. Phys.*, 11, 133–145, doi:10.5194/acp-11-133-2011, 2011.
- Environment and Climate Change Canada: Canadian Environmental Sustainability Indicators: Air Pollutant Emissions, Technical report, Environment and Climate Change Canada, ECCC Public Inquiries Centre, 200 Sacre-Coeur boul. Gatineau, QC, K1A 0H3, <http://www.ec.gc.ca/indicateurs-indicators/default.asp?lang=en&n=E79F4C12-1>, 2016.
- Environment and Climate Change Canada: Criteria air contaminants, Tech. rep., Environment and Climate Change Canada and Canadian Council of Ministers of the Environment, <https://www.ec.gc.ca/air/default.asp?lang=En&n=7C43740B-1>, last referenced 9 June 2017, 2017.
- 665 Fangmeier, A., Hadwiger-Fangmeier, A., der Eerden, L. V., and Jäger, H.-J.: Effects of atmospheric ammonia on vegetation—A review, *Environmental Pollution*, 86, 43 – 82, doi:http://dx.doi.org/10.1016/0269-7491(94)90008-6, 1994.
- Farquhar, G. D., Firth, P. M., Wetselaar, R., and Weir, B.: On the Gaseous Exchange of Ammonia between Leaves and the Environment Determination of the Ammonia Compensation Point, *Plant Physiol.*, 66, 710–714, doi:10.1104/pp.66.4.710, 1980.
- 670 Fu, X., Wang, S. X., Rau, L. M., Pleim, J. E., Cooter, E., Bash, J. O., Benson, V., and Hao, J. M.: Estimating NH₃ emissions from agricultural fertilizer application in China using the bi-directional CMAQ model coupled to an agro-ecosystem model, *Atmos. Chem. Phys.*, 15, 6637–6649, doi:10.5194/acp-15-6637-2015, 2015.



- Galloway, J. N., Townsend, A. R., Erisman, J. W., Bekunda, M., Cai, Z. C., Freney, J. R., Martinelli, L. A.,
675 Seitzinger, S. P., and Sutton, M. A.: Transformation of the nitrogen cycle: Recent trends, questions, and
potential solutions, *Science*, 320, 889–892, doi:10.1126/Science.1136674, 2008.
- Galperin, M. and Sofiev, M.: The long-range transport of ammonia and ammonium in the Northern Hemisphere,
Atmos. Environ., 32, 373 – 380, doi:10.1016/S1352-2310(97)00045-9, 1998.
- Giordano, L., Brunner, D., Flemming, J., Hogrefe, C., Im, U., Bianconi, R., Badia, A., Balzarini, A., Baró,
680 R., Chemel, C., Curci, G., Forkel, R., Jiménez-Guerrero, P., Hirtl, M., Hodzic, A., Hoznak, L., Jorba, O.,
Knote, C., Kuenen, J., Makar, P., Manders-Groot, A., Neal, L., Pérez, J., Pirovano, G., Pouliot, G., José,
R. S., Savage, N., Schröder, W., Sokhi, R., Syrakov, D., Torian, A., Tuccella, P., Werhahn, J., Wolke, R.,
Yahya, K., Zabkar, R., Zhang, Y., and Galmarini, S.: Assessment of the MACC reanalysis and its influence
as chemical boundary conditions for regional air quality modeling in AQMEII-2, *Atmos. Environ.*, 115,
685 371–388, doi:10.1016/j.atmosenv.2015.02.034, 2015.
- Gong, W., Makar, P. A., Zhang, J., Milbrandt, J., Gravel, S., Hayden, K. L., Macdonald, A. M., and Leaitch,
W. R.: Modelling aerosol cloud meteorology interaction: A case study with a fully coupled air quality model
GEM-MACH, *Atmos. Environ.*, 115, 695–715, doi:10.1016/j.atmosenv.2015.05.062, 2015.
- Gordon, M., Li, S.-M., Staebler, R., Darlington, A., Hayden, K., O'Brien, J., and Wolde, M.: Determining air
690 pollutant emission rates based on mass balance using airborne measurement data over the Alberta oil sands
operations, *Atmos. Meas. Tech.*, 8, 3745–3765, doi:10.5194/amt-8-3745-2015, 2015.
- Hansen, K., Personne, E., Skjoth, C. A., Loubet, B., Ibrom, A., Jensen, R., Sorensen, L. L., and Boegh, E.: In-
vestigating sources of measured forest-atmosphere ammonia fluxes using two-layer bi-directional modelling,
Agriculture and Forest Meteorology, 237–238, 20–94, doi:10.1016/j.agrformet.2017.02.008, 2017.
- 695 Heilman, W. E., Liu, Y., Urbanski, S., Kovalev, V., and Mickler, R.: Wildland fire emissions, carbon, and cli-
mate: Plume rise, atmospheric transport, and chemistry processes, *Forest Ecology and Management*, 317,
70 – 79, doi:http://dx.doi.org/10.1016/j.foreco.2013.02.001, wildland fire emissions, carbon, and climate:
Science overview and knowledge needs, 2014.
- Hsu, Y.-M. and Clair, T. A.: Measurement of fine particulate matter water-soluble inorganic species and precur-
700 sor gases in the Alberta Oil Sands Region using an improved semicontinuous monitor, *J. Air Waste Manage.*
Assoc., 65, 423–435, doi:10.1080/10962247.2014.1001088, 2015.
- Hsu, Y.-M. and Clair, T. A.: Measurement of fine particulate matter water-soluble inorganic species and precur-
sor gases in the Alberta Oil Sands Region using an improved semicontinuous monitor, *J. Air Waste Manage.*
Assoc., 568, 285–295, doi:10.1016/j.scitotenv.2016.05.205, 2016.
- 705 IPCC: Climate Change 2013: The Physical Science Basis, Contribution of Working Group I to the Fifth Assess-
ment Report of the Intergovernmental Panel on Climate Change, in: IPCC Fifth Assessment Report, edited
by Stocker, T. F., Qin, D., Plattner, G.-K., Tignor, M., Allen, S. K., Boschung, J., Nauels, A., Xia, Y., Bex,
V., and Midgley, P. M., Cambridge University Press, Cambridge, United Kingdom and New York, NY, USA,
2013.
- 710 Jimenez, J. L., Canagaratna, M. R., Donahue, N. M., and et al: Evolution of Organic Aerosols in the Atmo-
sphere, *Science*, 326, 1525–1529, doi:10.1126/science.1180353, 2009.



- Kelly, E. N., Short, J. W., Schindler, D. W., Hodson, P. V., Ma, M., Kwan, A. K., and Fortin, B. L.: Oil sands development contributes polycyclic aromatic compounds to the Athabasca River and its tributaries, *Proc. Natl. Acad. Sci.*, 106, 22 346–22 351, doi:10.1073/pnas.0912050106, 2009.
- 715 Kharol, S. K., Shephard, M. W., McLinden, C. A., Zhang, L., Sioris, C. E., Cady-Pereira, K. E., Vet, R., and Krotkov, N. A.: Satellite observations of reactive nitrogen (N_r) dry deposition from ammonia and nitrogen dioxide over North America, *Geophys. Res. Lett.*, in preparation, 2017.
- Kirk, J. L., Muir, D. C. G., Gleason, A., Wang, X., Lawson, G., Frank, R. A., Lehnerr, I., and Wrona, F.: Atmospheric Deposition of Mercury and Methylmercury to Landscapes and Waterbodies of the Athabasca
720 Oil Sands Region, *Environ. Sci. Technol.*, 48, 7374–7383, doi:10.1021/es500986r, 2014.
- Krupa, S.: Effects of atmospheric ammonia (NH_3) on terrestrial vegetation: a review, *Environmental Pollution*, 124, 179 – 221, doi:10.1016/S0269-7491(02)00434-7, 2003.
- Lamarque, J.-F., Bond, T. C., Eyring, V., Granier, C., Heil, A., Klimont, Z., Lee, D., Liousse, C., Mieville, A., Owen, B., Schultz, M. G., Shindell, D., Smith, S. J., Stehfest, E., Van Aardenne, J., Cooper, O. R., Kainuma,
725 M., Mahowald, N., Mc-Connell, J. R., Naik, V., Riahi, K., and van Vuuren, D. P.: Historical (1850–2000) gridded anthropogenic and biomass burning emissions of reactive gases and aerosols: methodology and application, *Atmos. Chem. Phys.*, 10, 7017–7039, doi:10.5194/acp-10-7017-2010, 2010.
- Larkin, N. K., O'Neill, S. M., Solomon, R., Raffuse, S., Strand, T., Sullivan, D., Krull, C., Rorig, M., Peterson, J., and Ferguson, S. A.: The BlueSky smoke modeling framework, *Int. J. Wildland Fire*, 18, 906–920,
730 doi:10.1071/WF07086, 2009.
- Lee, C. J., Martin, R. V., Henze, D. K., Brauer, M., Cohen, A., and van Donkelaar, A.: Response of Global particulate matter related mortality to changes in local precursor emissions, *Environ. Sci. and Tech.*, 49, 4335–4344, doi:10.1021/acs.est.5b00873, 2015.
- Li, S.-M., Leithead, A., Moussa, S. G., Liggio, J., Moran, M. D., Wang, D., Hayden, K., Darlington, A., Gordon,
735 M., Staebler, R., Makar, P. A., Stroud, C. A., McLaren, R., Liu, P. S. K., O'Brien, J., Mittermeier, R. L., Zhang, J., Marson, G., Cober, S. G., Wolde, M., and Wentzell, J. J. B.: Differences between measured and reported volatile organic compound emissions from oil sands facilities in Alberta, Canada, *Proc. Nat. Acad. Sci.*, doi:10.1073/pnas.1617862114, 2017.
- Liggio, J., Li, S.-M., Hayden, K., Taha, Y. M., Stroud, C., Darlington, A., Drollette, B. D., Gordon, M., Lee,
740 P., Liu, P., Leithead, A., Moussa, S. G., Wang, D., O'Brien, J., Mittermeier, R. L., Brook, J. R., Lu, G., Staebler, R. M., Han, Y., Tokarek, T. W., Osthoff, H. D., Makar, P. A., Zhang, J., L. Plata, D., and Gentner, D. R.: Oil sands operations as a large source of secondary organic aerosols, *Nature*, 534, 91–94, doi:10.1038/nature17646, 2016.
- Makar, P., Bouchet, V. S., and Nenes, A.: Inorganic chemistry calculations using HETV - a vectorized solver
745 for the SO_4^{2-} - NO_3^- - NH_4^+ system based on the ISORROPIA Algorithms, *Atmos. Environ.*, 37, 2279–2294, doi:10.5194/acp-9-7183-2009, 2003.
- Makar, P., Moran, M., Zheng, Q., Cousineau, S., Sassi, M., Duhamel, A., Besner, M., Davignon, D., Crevier, L.-P., and Bouchet, V. S.: Modelling the impacts of ammonia emissions reductions on North American air quality, *Atmos. Chem. Phys.*, 9, 7183–7212, doi:10.1016/S1352-2310(03)00074-8, 2009.
- 750 Makar, P., Gong, W., Hogrefe, C., Zhang, Y., Curci, G., Zabkar, R., Milbrandt, J., Im, U., Balzarini, A., Baró, R., Bianconi, R., Cheung, P., Forkel, R., Gravel, S., Hirtl, M., Honzak, L., Hou, A., Jiménez-Guerrero, P.,



- Langer, M., Moran, M., Pabla, B., Pérez, J., Pirovano, G., José, R. S., Tuccella, P., Werhahn, J., Zhang, J., and Galmarini, S.: Feedbacks between air pollution and weather, part 2: Effects on chemistry, *Atmos. Environ.*, 115, 499–526, doi:10.1016/j.atmosenv.2014.10.021, 2015a.
- 755 Makar, P. A., Gong, W., Milbrandt, J., Hogrefe, C., Zhang, Y., Curci, G., Zabkar, R. ., Im, U., Balzarini, A., Baró, R., Bianconi, R., Cheung, P., Forkel, R., Gravel, S., Hirtl, M., Honzak, L., Hou, A., Jiménez-Guerrero, P., Langer, M., Moran, M., Pabla, B., Pérez, J., Pirovano, G., José, R. S., Tuccella, P., Werhahn, J., Zhang, J., and Galmarini, S.: Feedbacks between air pollution and weather, part 1: Effects on weather, *Atmos. Environ.*, 115, 442–469, doi:10.1016/j.atmosenv.2014.12.003, 2015b.
- 760 Makar, P. A., Akingunola, A., Moran, M. D., Wong, I., Aherne, J., Hayden, K., Li, S. M., Zhang, J., Baratzehah, P., Pabla, B., Cheung, P., Cole, A., Kirk, J., Scott, K., and Zheng, Q.: Acid deposition simulations for Alberta, Saskatchewan, and the Canadian Oil Sands, using GEM-MACH, *Atmos. Chem. Phys.*, submitted to same ACP Oil Sands special issue, 2017.
- Massad, R.-S., Nemitz, E., and Sutton, M. A.: Review and parameterisation of bi-directional ammonia exchange between vegetation and the atmosphere, *Atmos. Chem. Phys.*, 10, 10359–10386, doi:10.5194/acp-10-10359-2010, 2010.
- Moran, M., Menard, S., Gravel, S., Pavlovic, R., and Anselmo, D.: RAQDPS Versions 1.5.0 and 1.5.1: Upgrades to the CMC Operational Regional Air Quality Deterministic Prediction System Released in October 2012 and February 2013, Technical report, Canadian Meteorological Centre, Canadian Meteorological Centre, 770 Dorval, Quebec, 2013.
- Moran, M., Zheng, Q., Zhang, J., and Pavlovic, R.: RAQDPS Version 013: Upgrades to the CMC Operational Regional Air Quality Deterministic Prediction System Released in June 2015, Technical report, Canadian Meteorological Centre, Canadian Meteorological Centre, Dorval, Quebec, 2015.
- Moran, M. D., Ménard, S., Talbot, D., Huang, P., Makar, P. A., Gong, W., Landry, H., Gravel, S., Gong, S., 775 Crevier, L.-P., Kallaur, A., and Sassi, M.: Particulate-matter forecasting with GEM-MACH15, a new Canadian air-quality forecast model, in: *Air pollution modelling and its application XX*, edited by Steyn, D. G. and Rao, S. T., pp. 289–292, Springer, Dordrecht, 2010.
- Moss, R. H., Edmonds, J. A., Hibbard, K. A., Manning, M. R., Rose, S. K., van Vuuren, D. P., Carter, T. R., Emori, S., Kainuma, M., Kram, T., Meehl, G. A., Mitchell, J. F. B., Nakicenovic, N., Riahi, K., Smith, S. J., 780 Stouffer, R. J., Thomson, A. M., Weyant, J. P., and Wilbanks, T. J.: The next generation of scenarios for climate change research and assessment, *Nature*, 463, 747–756, doi:10.1038/nature08823, 2010.
- Nemitz, E., Sutton, M. A., Schjoerring, J. K., Husted, S., and Wyers, G. P.: Resistance modelling of ammonia exchange over oilseed rape, *Agr. For. Meteorol.*, 105, 405–425, doi:10.1016/S0168-1923(00)00206-9, 2000.
- Nemitz, E., Milford, C., and Sutton, M. A.: A two-layer canopy compensation point model for describing bi-directional biosphere-atmosphere exchange of ammonia, *Q. J. Roy. Meteorol. Soc.*, 127, 815–833, 785 doi:10.1002/qj.49712757306, 2001.
- Nenes, A., Pilinis, C., and Pandis, S.: ISORROPIA: A New Thermodynamic Model for Multiphase Multicomponent Inorganic Aerosols, *Aquat. Geochem.*, 4, 123–152, doi:10.1023/A:1009604003981, 1998.
- Olivier, J., Bouwman, A., der Hoek, K. V., and Berdowski, J.: Global air emission inventories for anthropogenic sources of NO_x, NH₃ and N₂O in 1990, *Environmental Pollution*, 102, 135 – 148, 790 doi:[http://dx.doi.org/10.1016/S0269-7491\(98\)80026-2](http://dx.doi.org/10.1016/S0269-7491(98)80026-2), 1998.



- Park, R. J., Jacob, D. J., Field, B. D., Yantosca, R. M., and Chin, M.: Natural and transboundary pollution influences on sulfate-nitrate-ammonium aerosols in the United States: Implications for policy, *J. Geophys. Res.*, 109, doi:10.1029/2003JD004473, d15204, 2004.
- 795 Paugam, R., Wooster, M., Freitas, S., and Val Martin, M.: A review of approaches to estimate wildfire plume injection height within large-scale atmospheric chemical transport models, *Atmos. Chem. Phys.*, 16, 907–925, doi:10.5194/acp-16-907-2016, 2016.
- Paulot, F., Jacob, D. J., Pinder, R. W., Bash, J. O., Travis, K., and Henze, D. K.: Ammonia emissions in the United States, European Union, and China derived by high-resolution inversion of ammonium wet deposition data: Interpretation with a new agricultural emissions inventory (MASAGE NH₃), *J. Geophys. Res.*, 119, 4343–4364, doi:10.1002/2013JD021130, 2014.
- 800 Pavlovic, R., Chen, J., Anderson, K., Moran, M., Beaulieu, P.-A., Davignon, D., and Cousineau, S.: The Fire-Work air quality forecast system with near-real-time biomass burning emissions: Recent developments and evaluation of performance for the 2015 North American wildfire season, *J. Air Waste Manage. Assoc.*, 66, 819–841, doi:10.1080/10962247.2016.1158214, 2016.
- 805 Pleim, J. E., Bash, J. O., Walker, J. T., and Cooter, E. J.: Development and evaluation of an ammonia bidirectional flux parameterization for air quality models, *J. Geophys. Res.*, 118, 3794–3806, doi:10.1002/jgrd.50262, 2013.
- Pope III, C., Burnett, R., Thun, M., and et al: Lung cancer, cardiopulmonary mortality, and long-term exposure to fine particulate air pollution, *JAMA*, 287, 1132–1141, doi:10.1001/jama.287.9.1132, 2002.
- 810 Robichaud, A.: Statistical links between meteorological factors and tropospheric ozone levels at the Duchesnay forest site, *Climat*, 12, 31–57, 1994.
- Robichaud, A. and Lin, C. A.: The linear steady response of a stratified baroclinic atmosphere to elevated diabatic forcing, *Atmosphere - Ocean*, 29, 619–635, doi:10.1080/07055900.1991.9649421, 1991.
- 815 Rogers, C. D.: *Inverse methods for atmospheric Sounding: Theory and Practice*, World Sci., Hackensack, NJ, 2000.
- Rooney, R. C., Bayley, S. E., and Schindler, D. W.: Oil sands mining and reclamation cause massive loss of peatland and stored carbon, *Proc. Natl. Acad. Sci.*, 109, 4933–4937, doi:10.1073/pnas.1117693108, 2012.
- Seinfeld, J. H. and Pandis, S. N., eds.: *Atmospheric Chemistry and Physics: From Air Pollution to Climate Change*, Wiley-Intersci., New York, 1326 pp., 1998.
- 820 Shephard, M. W. and Cady-Pereira, K. E.: Cross-track Infrared Sounder (CrIS) satellite observations of tropospheric ammonia, *Atmos. Meas. Techn.*, 8, 1323–1336, doi:10.5194/amt-8-1323-2015, 2015.
- Shephard, M. W., Cady-Pereira, K. E., Luo, M., Henze, D. K., Pinder, R. W., Walker, J. T., Rinsland, C. P., Bash, J. O., Zhu, L., Payne, V. H., and Clarisse, L.: TES ammonia retrieval strategy and global observations of the spatial and seasonal variability of ammonia, *Atmos. Chem. Phys.*, 11, 10743–10763, doi:10.5194/acp-11-10743-2011, 2011.
- 825 Shephard, M. W., McLinden, C. A., Cady-Pereira, K. E., Luo, M., Moussa, S. G., Leithead, A., Liggio, J., Staebler, R. M., Akingunola, A., Makar, P., Lehr, P., Zhang, J., Henze, D. K., Millet, D. B., Bash, J. O., Zhu, L., Wells, K. C., Capps, S. L., Chaliyakunnel, S., Gordon, M., Hayden, K., Brook, J. R., Wolde, M., and Li, S.-M.: Tropospheric Emission Spectrometer (TES) satellite observations of ammonia, methanol, formic acid,
- 830



- and carbon monoxide over the Canadian oil sands: validation and model evaluation, *Atmos. Meas. Tech.*, 8, 5189–5211, doi:10.5194/amt-8-5189-2015, 2015.
- Shinozuka, Y., Redemann, J., Livingston, J. M., Russell, P. B., Clarke, A. D., Howell, S. G., Freitag, S., O'Neill, N. T., Reid, E. A., Johnson, R., Ramachandran, S., McNaughton, C. S., Kapustin, V. N., Brekhovskikh, V., Holben, B. N., and McArthur, L. J. B.: Airborne observation of aerosol optical depth during ARC-TAS: vertical profiles, inter-comparison and fine-mode fraction, *Atmos. Chem. Phys.*, 11, 3673–3688, doi:10.5194/acp-11-3673-2011, 2011.
- 835 Sutton, M., Milford, C., Dragosits, U., Place, C., Singles, R., Smith, R., Pitcairn, C., Fowler, D., Hill, J., ApSimon, H., Ross, C., Hill, R., Jarvis, S., Pain, B., Phillips, V., Harrison, R., Moss, D., Webb, J., Espenhahn, S., Lee, D., Hornung, M., Ulliyett, J., Bull, K., Emmett, B., Lowe, J., and Wyers, G.: Dispersion, deposition and impacts of atmospheric ammonia: quantifying local budgets and spatial variability, *Environmental Pollution*, 102, 349 – 361, doi:[http://dx.doi.org/10.1016/S0269-7491\(98\)80054-7](http://dx.doi.org/10.1016/S0269-7491(98)80054-7), 1998.
- 840 Sutton, M. A., Fowler, D., and Moncrieff, J. B.: The Exchange of Atmospheric Ammonia with Vegetated Surfaces .1. Unfertilized Vegetation, *Q. J. Roy. Meteorol. Soc.*, 119, 1023–1045, doi:10.1002/qj.49711951309, 1993.
- 845 Sutton, M. A., Schjorring, J. K., and Wyers, G. P.: Plant Atmosphere Exchange of Ammonia, *Philos. T. Roy. Soc. A.*, 351, 261–276, <http://www.jstor.org/stable/54415>, 1995.
- Urbanski, S.: Wildland fire emissions, carbon, and climate: Emission factors, *Forest Ecology and Management*, 317, 51–60, doi:10.1016/j.foreco.2013.05.045, 2014.
- 850 Van Damme, M., Clarisse, L., Heald, C. L., Hurtmans, D., Ngadi, Y., Clerbaux, C., Dolman, A. J., Erisman, J. W., and Coheur, P. F.: Global distributions, time series and error characterization of atmospheric ammonia (NH₃) from IASI satellite observations, *Atmos. Chem. Phys.*, 14, 2905–2922, doi:10.5194/acp-14-2905-2014, 2014.
- Wen, D., Zhang, L., Lin, J. C., Vet, R., and Moran, M. D.: An evaluation of ambient ammonia concentrations over southern Ontario simulated with different dry deposition schemes within STILT-Chem v0.8, *Geosci. Model Dev.*, 7, 1037–1050, doi:10.5194/gmd-7-1037-2014, 2014.
- 855 Wentworth, G. R., Murphy, J. G., Willis, M. D., Lee, M. K. Y., Abbat, J. P. D., Li, S.-M., Brook, J. R., Makar, P., Akingunola, A., and Whaley, C.: Ammonia and particle acidity in the Athabasca Oil Sands Region, tbd, tbd, doi:tbd, 2017.
- 860 Wesely, M. L.: Parameterization of surface resistances to gaseous dry deposition in regional-scale numerical models, *Atmos. Environ.*, 23, 1293–1304, doi:10.1016/0004-6981(89)90153-4, 1989.
- Wichink Kruit, R., van Pul, W., Sauter, F., van den Broek, M., Nemitz, E., Sutton, M., Krol, M., and Holtslag, A.: Modeling the surface–atmosphere exchange of ammonia, *Atmos. Environ.*, 44, 945 – 957, doi:10.1016/j.atmosenv.2009.11.049, 2010.
- 865 Wu, Y., Walker, J., Schwede, D., Peters-Lidard, C., Dennis, R., and Robarge, W.: A new model of bi-directional ammonia exchange between the atmosphere and biosphere: Ammonia stomatal compensation point, *Agr. Forest Meteorol.*, 149, 263 – 280, doi:10.1016/j.agrformet.2008.08.012, 2009.
- Zhang, J., Moran, M. D., Zheng, Q., Makar, P. A., Baratzadeh, P., Marsen, G., Liu, P., and Li, S.-M.: Emissions preparation and analysis for multiscale air quality modelling over the Athabasca oil sands region of Alberta, Canada, *Atmos. Chem. Phys.*, submitted to same ACP Oil Sands special issue, 2017.
- 870

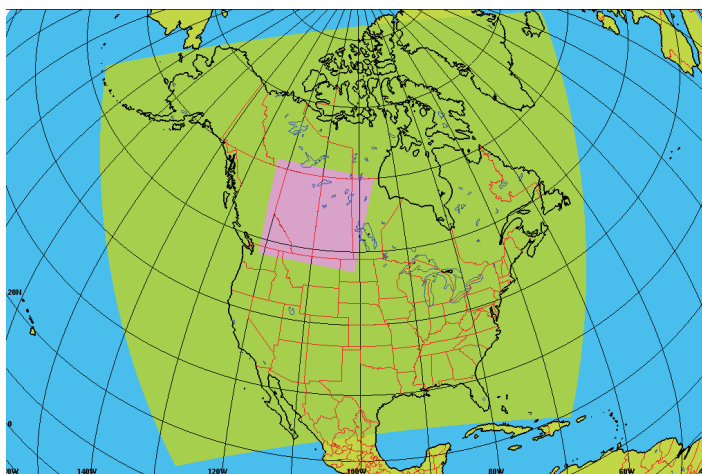


Figure 1. Map of 10-km resolution continental piloting model domain (green), and 2.5-km resolution nested model domain (purple).

Zhang, L., Moran, M., Makar, P., Brook, J., and Gong, S.: Gaseous Dry Deposition in AURAMS A Unified Regional Air-quality Modelling System, *Atmos. Environ.*, 36, 537–560, doi:10.1016/S1352-2310(01)00447-2, 2002.

Zhang, L., Brook, J. R., and Vet, R.: A revised parametrization for gaseous dry deposition in air-quality models, *Atmos. Chem. Phys.*, 3, 2067–2082, doi:10.5194/acp-3-2067-2003, 2003.

Zhang, L., Wright, L. P., and Asman, W. A. H.: Bi-directional air-surface exchange of atmospheric ammonia: A review of measurements and a development of a big-leaf model for applications in regional-scale air-quality models, *J. Geophys. Res.*, 115, D20 310, doi:10.1029/2009JD013589, 2010.

Zhu, L., Henze, D. K., Cady-Pereira, K. E., Shephard, M. W., Luo, M., Pinder, R. W., Bash, J. O., and Jeong, G.-R.: Constraining U.S. ammonia emissions using TES remote sensing observations and the GEOS-Chem adjoint model, *J. Geophys. Res.*, 118, 3355–3368, doi:10.1002/jgrd.50166, 2013.

Zhu, L., Henze, D., Bash, J., Jeong, G.-R., Cady-Pereira, K., Shephard, M., Luo, M., Paulot, F., and Capps, S.: Global evaluation of ammonia bidirectional exchange and livestock diurnal variation schemes, *Atmos. Chem. Phys.*, 15, 12 823–12 843, doi:10.5194/acp-15-12823-2015, 2015.

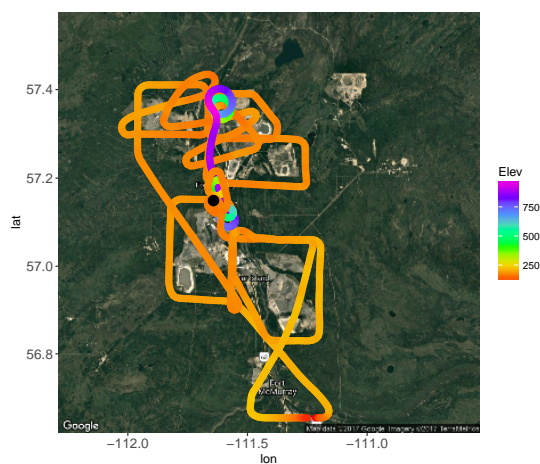


Figure 2. Flight path on 13 August 2013, where elevation (in meters) is denoted by the colour scale, and the AMS13 site is indicated by a black circle.

Table 1. Latitude and longitude ranges that the model was evaluated over with the CrIS satellite measurements

domain	date (in 2013)	lat range (°)	lon range (°)
AB/SK large domain	12 Aug to 7 Sept	48 to 60 N	-122.0 to -100.0 W
northern, no-fire case study	3 Sept	55 to 60 N	-120.0 to -110.0 W
southern, no-fire case study	1 Sept	49 to 53.5 N	-117.0 to -106.0 W
northern, fire case study	12 Aug	56.5 to 60 N	-110.0 to -104.4 W

Table 2. Average source contributions to ambient NH_3 concentrations over the AB/SK model domain during 12 Aug to 7 Sep 2013.

source	median (ppbv)	median (%)	average (ppbv)	average (%)
total surface NH_3	1.60	100	2.53	100
from fires to surface	0.25	10.4	0.42	20.3
from bidi to surface	0.97	56.3	1.24	56.6
from anthro to surface	0.38	33.3	0.87	23.1
total column NH_3	18.8	100	25.6	100
from fires to total column	6.1	27.7	8.1	30.5
from bidi to total column	8.8	48.1	11.15	50.0
from anthro to total column	3.9	24.2	6.35	19.5

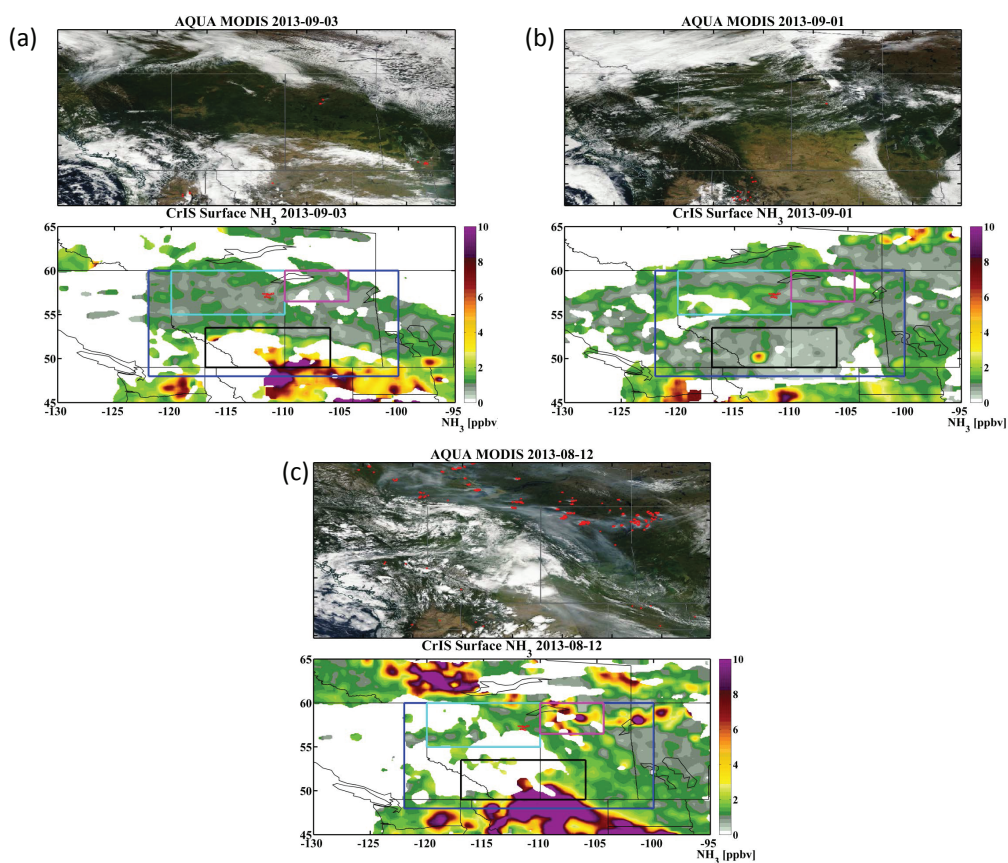


Figure 3. (Top panels) Images of the Alberta/Saskatchewan region with clouds and fire hotspots from MODIS. (Bottom panels) Map of CrIS-measured surface NH₃ concentrations, with coloured boxes showing the regions where model and satellite measurements were sampled. These three examples are for (a) northern bidi case study (cyan), (b) southern bidi case study (black), and (c) fire case study (magenta), discussed in Section 4.3, and the blue box is the region of our overall comparison.

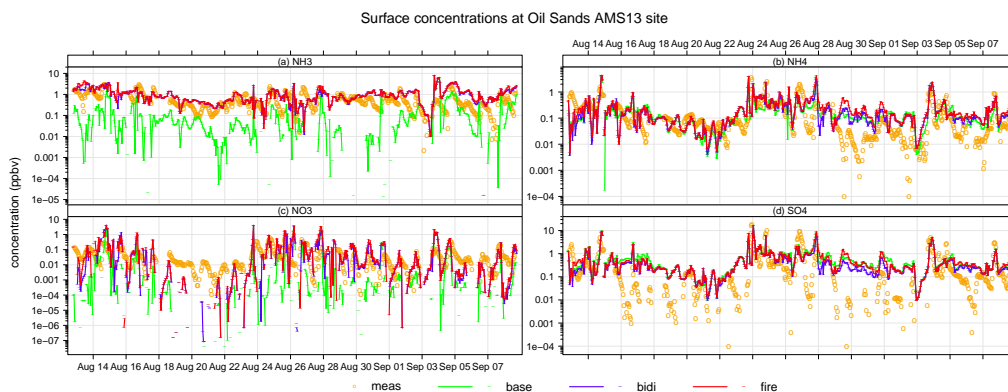


Figure 4. Surface (a) NH_3 , (b) fine particulate NH_4^+ , (c) NO_3^- , and (d) SO_4^{2-} concentrations at the AMS13 ground site in the AOSR. Measurements in orange, base model in green, bidirectional flux model in blue, and fire+bidi model in red. Y-scale is logarithmic.

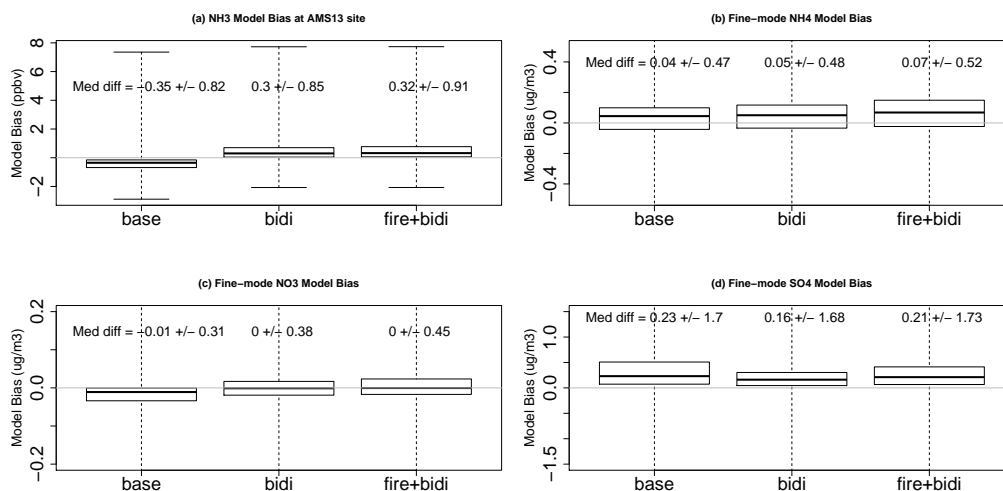


Figure 5. Model-measurement bias in surface (a) NH_3 , (b) NH_4^+ , (c) NO_3^- and (d) SO_4^{2-} concentrations at the AMS13 ground site in the AOSR.

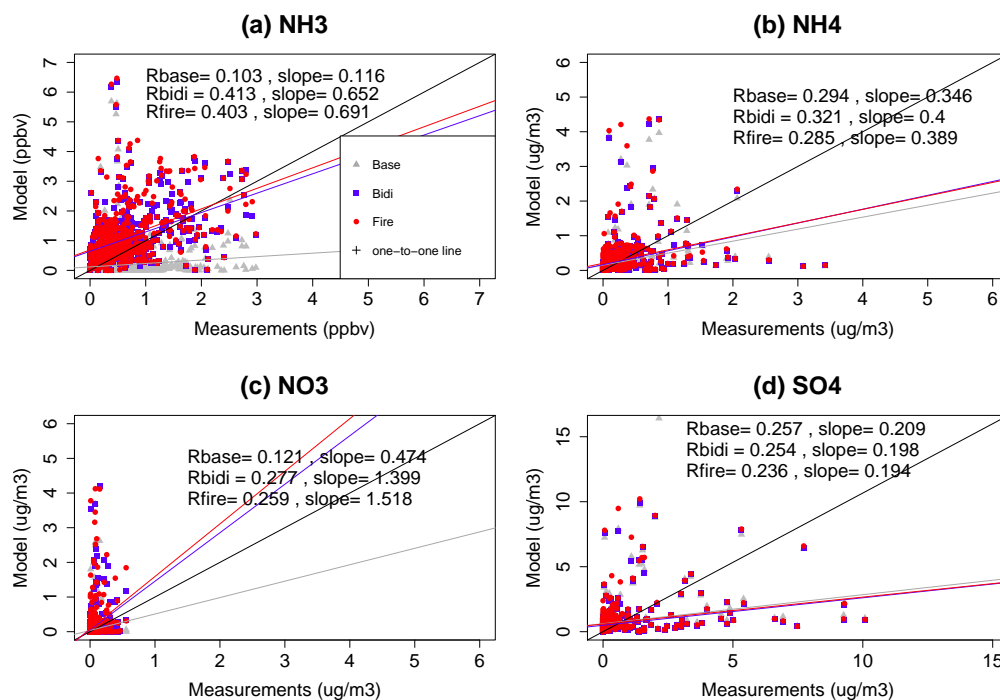


Figure 6. Modelled vs measured surface (a) NH₃, (b) NH₄⁺, (c) NO₃⁻ and (d) SO₄²⁻ concentrations at the AMS13 ground site in the AOSR. Base model in grey, bidirectional flux model in blue, and fire+bidi model in red.

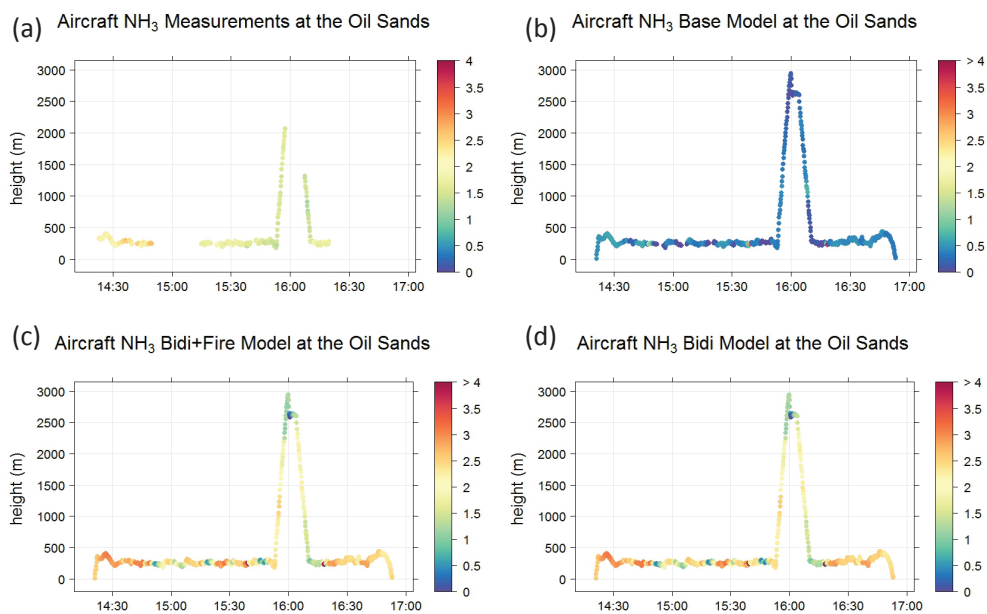


Figure 7. NH_3 concentrations aloft (colour scale) over the OS region during the 13 August 2013 flight. (a) measurements, (b) base model, (c) fire+bidi model, and (d) bidi model.

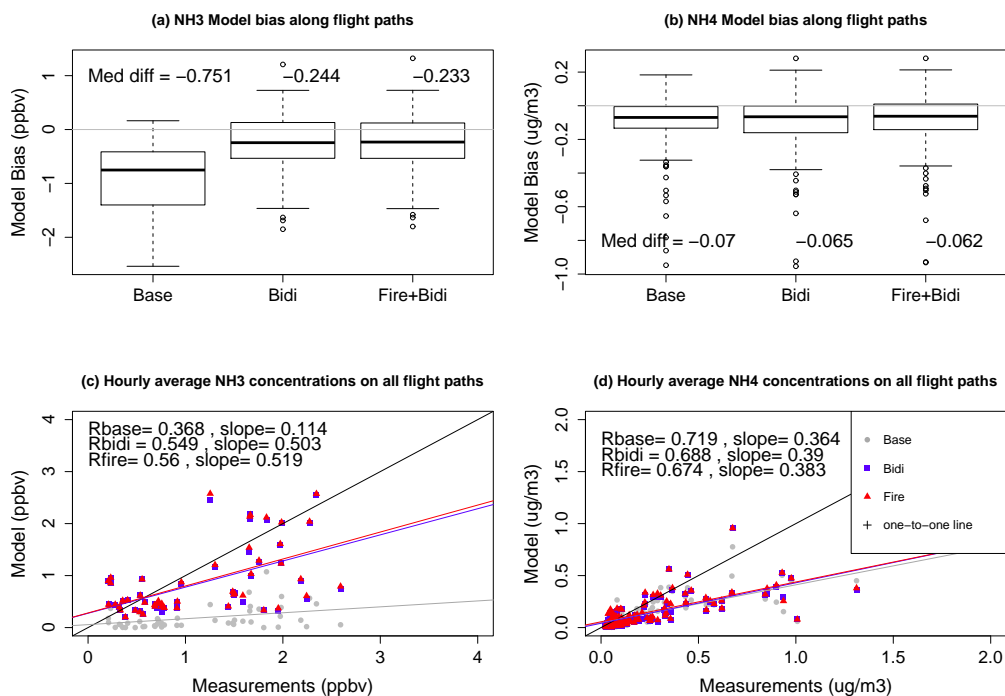


Figure 8. Hourly averages along all flight paths over the OS region during the summer 2013 campaign: Model-measurement bias in (a) NH₃ and (b) NH₄⁺. Modelled vs measured (c) NH₃ and (d) NH₄⁺ concentrations aloft. Base model in grey, bidirectional flux model in blue, and fire+bidi model in red.

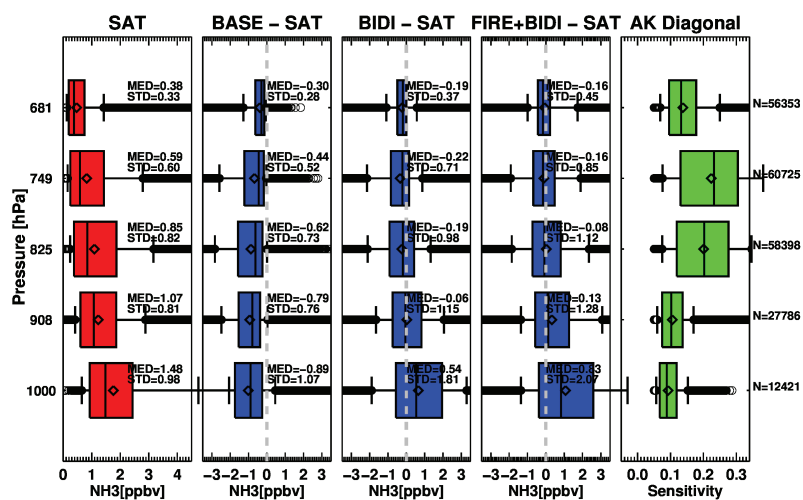


Figure 9. (a) NH_3 vertical profile as measured by CrIS satellite, difference between measurement and (b) base model, (c) bidi model, and (d) fire+bidi model, and (e) averaging kernel of CrIS satellite for NH_3 retrieval.

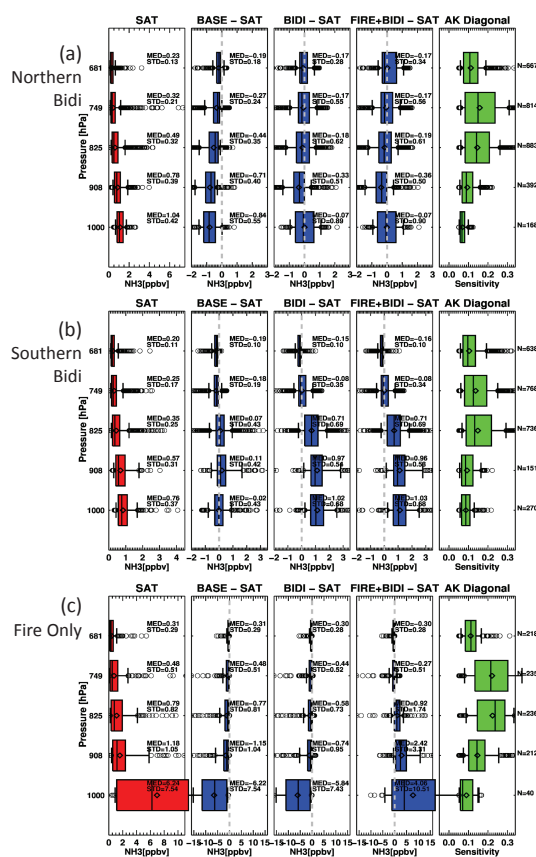


Figure 10. As in Fig. 9, but for our (a) northern “bidi-only” case study (3 Sept 2013), (b) southern “bidi-only” case study (1 Sept 2013), and (c) northern “fire-only” case study (12 Aug 2013). Regions are shown in Figure 3a (cyan), 3b (black), and 3c (magenta) boxes, respectively).

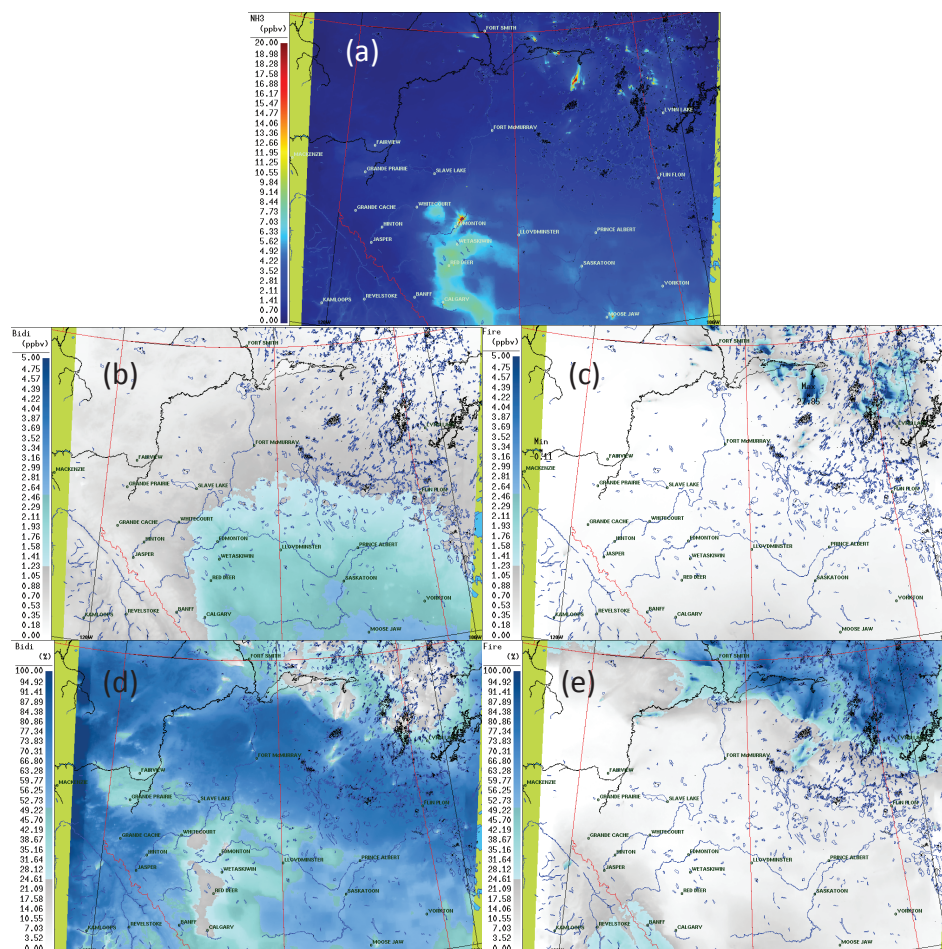


Figure 11. Maps of the modelled average (a) surface NH_3 concentrations (b) absolute bidirectional flux contribution, (c) absolute fire contribution, (d) percent bidirectional flux contribution, and (e) percent fire contribution to surface NH_3 . These are averaged over 12 August to 7 September, 2013.

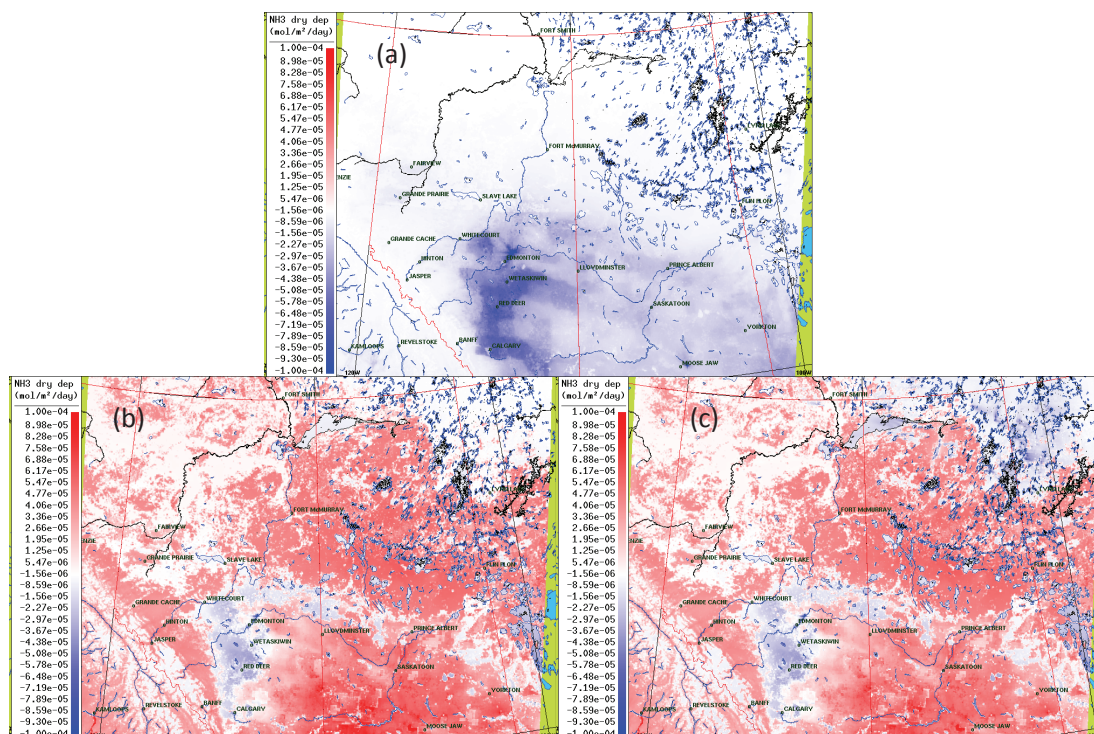


Figure 12. Maps of the modelled average NH_3 dry deposition for (a) base (b) bidi, and (c) fire+bidi models. In all maps, red/positive represents upward flux, and blue/negative represents downward flux. These are daily amounts, averaged over 12 August to 7 September, 2013.

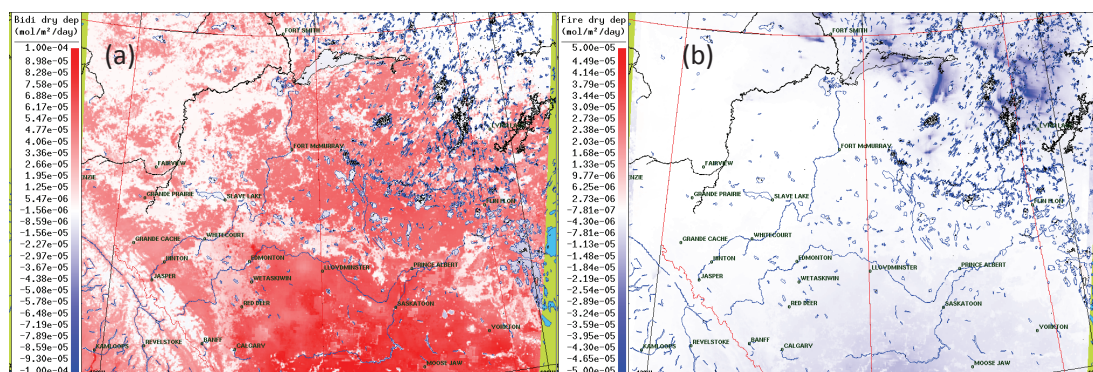


Figure 13. Maps modelled daily average (a) bidi and (b) fire components to dry deposition. In all maps, red/positive represents upward flux, and blue/negative represents downward flux. These are daily amounts, averaged over 12 August to 7 September, 2013.

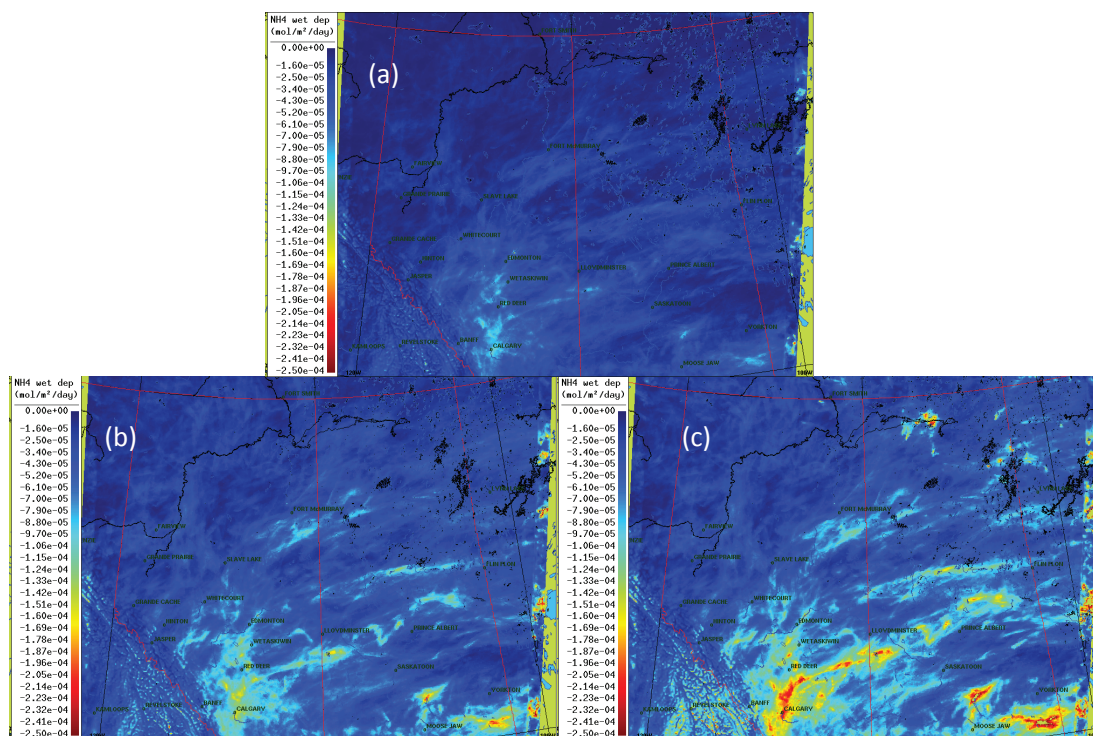


Figure 14. Maps of the modelled average NH_4^+ wet deposition for (a) base (b) bidi, and (c) fire+bidi models. Negative represents downward flux. These are daily amounts, averaged over 12 August to 7 September, 2013.